**Investigation on the Kinematics of Entrapped Air Pockets in Stormwater Storage Tunnels**

by

Carmen Chosie

A thesis submitted to the Graduate Faculty of
Auburn University
in partial fulfillment of the
requirements for the Degree of
Master of Science

Auburn, Alabama
December 14, 2013

Keywords: Stormwater tunnels; Air pockets; Laboratory experiments



Approved by

Jose G. Vasconcelos, Chair, Assistant Professor of Civil Engineering
Prabhakar Clement, Professor of Civil Engineering
Xing Fang, Associate Professor of Civil Engineering

Abstract

Various mechanisms can lead to the entrapment of air pockets within stormwater storage tunnels when they undergo rapid filling during intense rain events [Vasconcelos and Wright(2006)]. These entrapped air pockets are linked to operational issues within systems such as damaging surges, storage capacity loss, and severe geysering upon their release through water-filled ventilation shafts. Therefore, tracking entrapped air pockets and their celerity is important in the context of numerical simulation to assess the risk of the aforementioned operational issues. Previous studies focused on quantifying the magnitude of pressure surges associated with air pocket compression or in obtaining the minimum flow velocities required to expel the entrapped air pockets from water mains (hydraulic clearing). However, the conditions controlling the motion of these finite volume pockets following entrapment require further investigation. A balance between drag and buoyancy forces is expected to control the motion of discrete air pockets in closed conduits, yet there have been limited studies in terms of how factors such as varying pipeline slope, background flow, and air pocket volume affect air pocket motion. This research aims to explore a link between ambient flow velocity, pipeline slope, and the celerity of entrapped air pockets of various volumes. This work presents experimental results from an investigation on the kinematics of entrapped air pockets in pressurized water flows under various shallow slopes (up to 2% favorable and adverse). Results of pocket trajectories and celerities are systematically compared for various tested slopes, flow rates, and pocket volumes. These experimental results are useful for the future development of numerical models that can include the motion of entrapped air pockets in closed conduits.

Acknowledgments

I would like to thank my professor and advisor, Professor Jose Vasconcelos, for his time and patience spent in the development of my experimental research as well as writing conference papers, monographs, and this thesis. I also would like to thank Amanda Summers, Holly Guest, and Andrew Patrick for all their hands-on help in the laboratory. I would also like to acknowledge the support provided by LimnoTech Inc. and Auburn University which has funded part of this research.

I would like to thank my parents, Dr. Kim and Mr. Kern Clark, who have always supported my motivation and drive to keep learning. Without their sacrifices and gifts, I would not have been able to complete both my degrees at Auburn University. My fiance, Nick, deserves much thanks for putting up with all my late nights of stress and offering to buy me ice cream and chocolate.

Finally, I am also thankful for all my friends in the civil engineering department who made classes, lab work and writing a great experience. These include: Holly Guest, Kristi and Tyler Mitchell, Jacob Kearley, Andrew Patrick, Kyle Moynihan, Tom Hatcher, Mitchell Moore, Catherine Butler, and Farhad Jazaei.

Table of Contents

List of Figures

List of Tables

List of Abbreviations

| | |
|---|---|
| $A$ | Pipeline area=$\frac{\pi}{4}D^2$ |
| $C$ | Celerity |
| $C^*$ | Normalized celerity=$\frac{C}{\sqrt{gD}}$ |
| $D$ | Pipeline diameter |
| $g$ | Gravitational acceleration |
| $L$ | Pipeline length |
| $L^1$ | Location along pipeline length=$\frac{X}{L}$ |
| $Q$ | Flow rate in the pipeline |
| $Q^*$ | Normalized flow rate in the pipeline=$Q/\sqrt{gD^5}$ |
| $t$ | Time |
| $t^*$ | Normalized time=$\frac{t}{\sqrt{\frac{D}{g}}}$ |
| $v_{flow}$ | Flow velocity |
| $v^*_{flow}$ | Normalized flow velocity=$\frac{v_{flow}}{\sqrt{gD}}$ |
| $Vol$ | Air pocket volume |
| $Vol^*$ | Normalized air pocket volume=$Vol/D^3$ |
| $X$ | Location along pipeline length |
| $X^*$ | Normalized location along pipeline length=$\frac{X}{X_0}$ |

$X_0$ Initial air pocket length=2.1 m

# Chapter 1

# Introduction

Deep storage tunnels have been utilized in highly urbanized areas as the means to provide relief to the stormwater collection systems during intense rain events as well as treatment to runoff. Operational problems such as damaging pressure surges and geysering episodes in these systems led to investigations with the goal of identifying the causes of these problems, which have been observed when these tunnels undergo rapid filling during intense rain events. The role of entrapped air pockets and the problems associated with these pockets is currently being identified by recent investigations. Evidence suggests that the entrapped air pockets have major impacts in system behavior relating to pressure surges magnitudes, loss of storage capacity, an geysering. A better understanding of air pocket behavior is required so that better design guidelines can be developed and implemented to avoid these adverse conditions.

## 1.1 Mechanisms for air pocket entrapment

Rapid filling of closed pipes can lead to the entrapment of air pockets through many different mechanisms, which depend entirely on the type of hydraulic system under consideration. There are various contexts in which air in closed conduits creates an issue, which arise from the fact that these conveyance systems are not designed to operate in two-phase flows. Various causes for air entrainment in transmission mains have been identified to date, and a comprehensive summary is presented by [Lauchlan et al(2005)]. These mechanisms include 1) entrainment at inflow (drop chamber, inlet, or intake) and outflow (outfalls in tidal areas placed above sea level) locations; 2) entrainment due to vortices, turbulence and hydraulic jumps; 3) insufficient pump submergence; 4) filling or emptying of pipelines; and

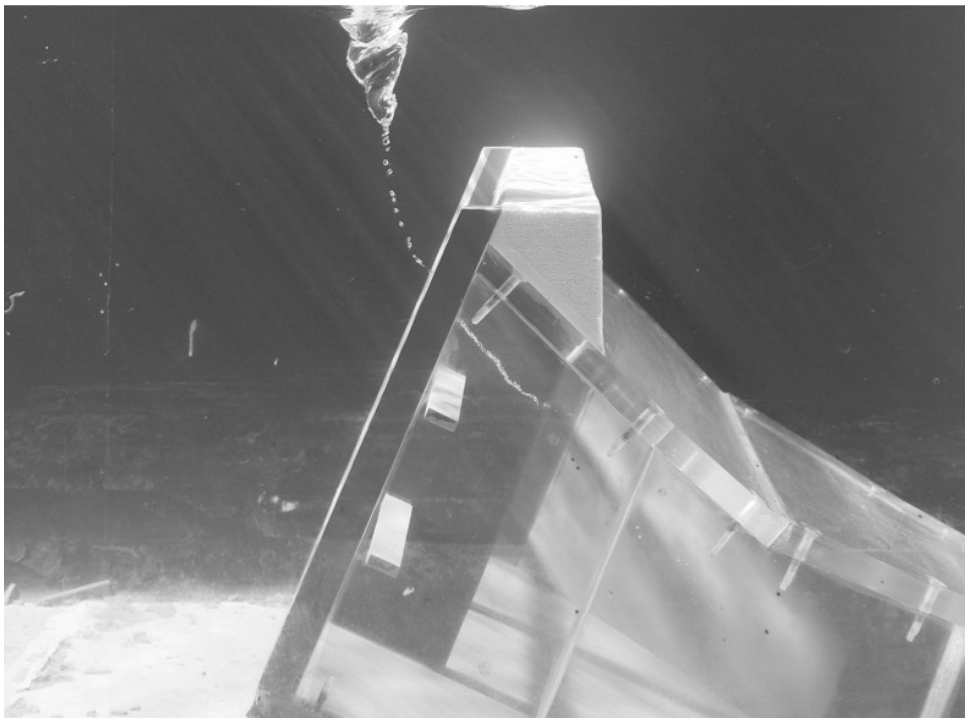

Figure 1.1: Air entraining vortex at intake structure due to insufficient pump submergence [Pinott and Moller(2011)].

5) negative pressures at the pipe inlet. Figure 1.1 displays an air entraining vortex at an intake structure due to insufficient pump submergence.

Other mechanisms have been identified in the context of the filling of stormwater systems. An early study by [Hamam and McCorquodale(1982)] indicates that interface stability caused by the relative motion between air and water can lead to surface waves in water that can grow and eventually promote an air pocket entrapment. This and other mechanisms for air pocket entrapment in the context of stormwater systems have been studied experimentally by [Vasconcelos and Wright(2006)], which also includes mechanisms such as insufficient (see Figure 1.2) or misplaced ventilation (Figure 1.3), breakdown of pressurization air-water interfaces (Figure 1.4), air-water shear flow instabilities (Figure 1.5), and gradual flow regime transition (GRFT) as shown in Figure 1.6.

Figure 1.7 displays an air pocket formation mechanism observed during a numerical simulation of an actual rapid filling scenario. The reflection of an inflow front from the

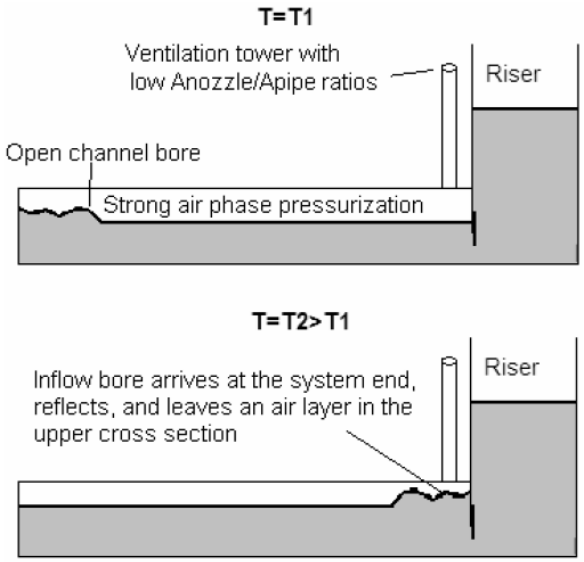


Figure 1.2: Pocket entrapment due to inadequate ventilation [Vasconcelos and Wright(2006)].

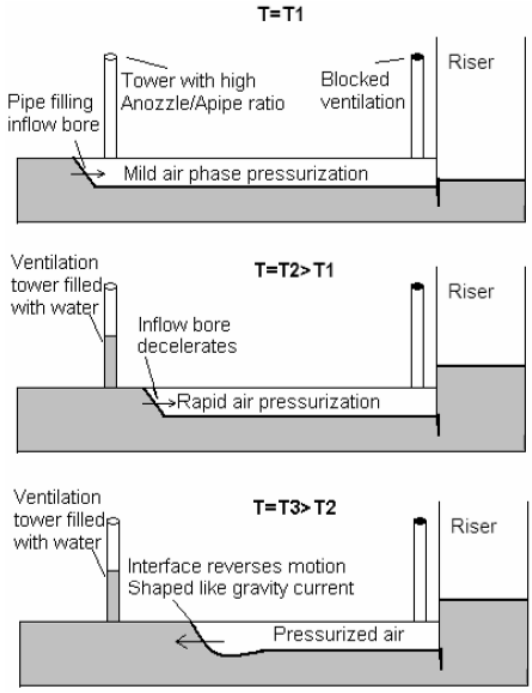


Figure 1.3: Pocket entrapment due to misplaced ventilation [Vasconcelos and Wright(2006)].

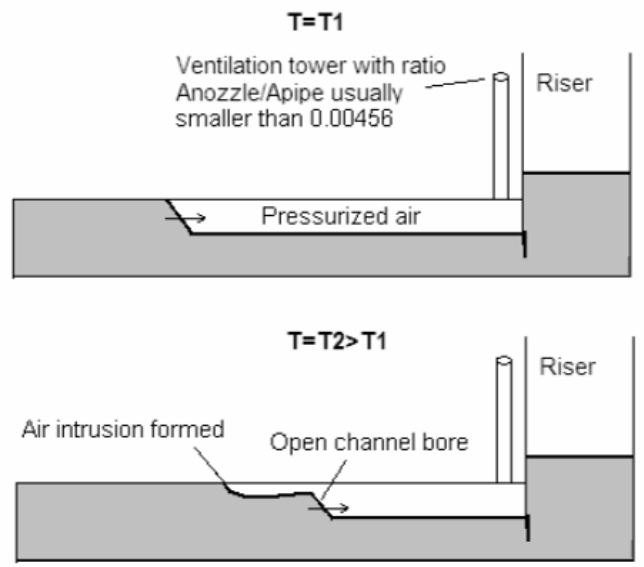


Figure 1.4: Pocket entrapment due to interface breakdown [Vasconcelos and Wright(2006)].

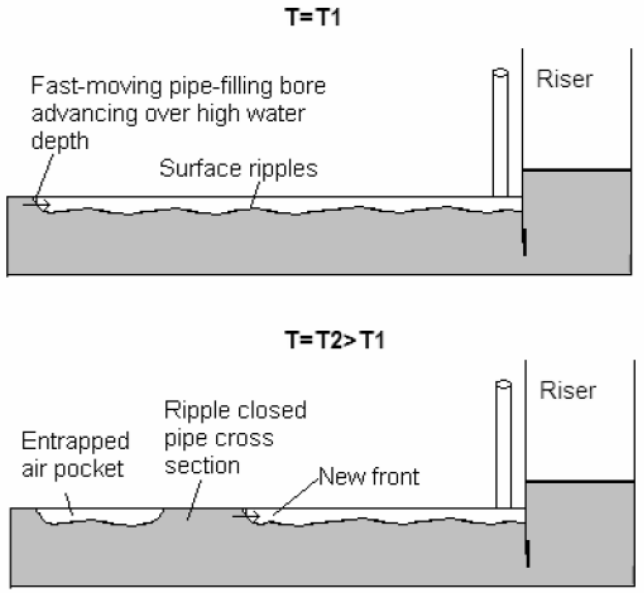


Figure 1.5: Pocket entrapment due to shear flow instability [Vasconcelos and Wright(2006)].

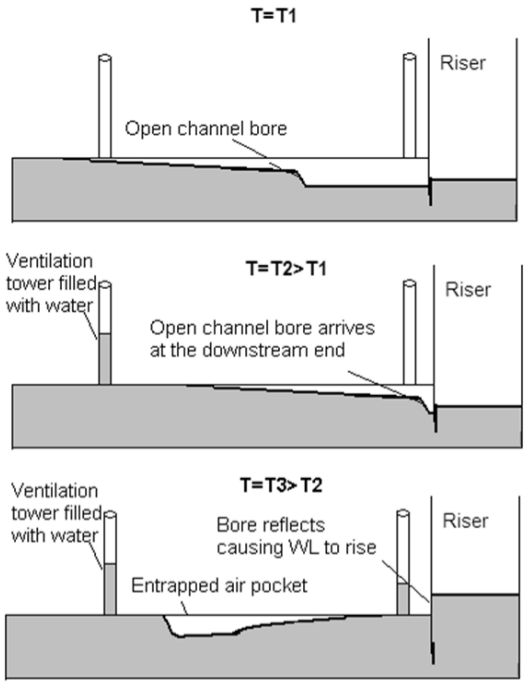


Figure 1.6: Pocket entrapment due to GFRT [Vasconcelos and Wright(2006)].

system boundary entraps air forming a large pocket at this location. This is a potentially harmful condition if this pocket is evacuated through a water-filled ventilation pipe, an event that can only be assessed by learning more about the kinematics of entrapped air pockets. More studies related to the formation and motion of air in stormwater systems are illustrated by [Hamam and McCorquodale(1982)], [Li and McCorquodale(1999)], [Zhou et al(2002)] and [Lautenbach et al(2008)]. While relevant, these studies do not provide means to track the location of discrete entrapped air pockets to assess likelihood and attempt prevention of deleterious air-water interactions.

## 1.2 Studies on gravity currents

Other related areas of investigation to those involving air-water flow in closed conduits include the propagation of gravity currents, particularly the case of non-Boussinesq currents

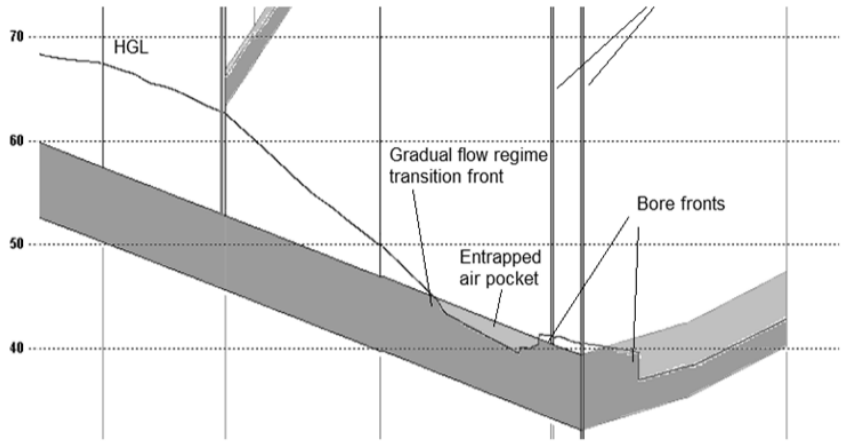


Figure 1.7: Air pocket entrapment mechanism related to the reflection of inflow fronts from the system boundary [Vasconcelos and Leite(2012)].

such as the intursion of an air cavity in a pipe initially filled with water. Classical contributions in fluid mechanics in this area are exemplified in the works by [Zukoski (1966)], [Benjamin(1968)], [Wilkinson(1982)], [Baines(1991)], and [Simpson(1997)] among others. Such air cavities are referred to as gravity currents in this context. Unlike cases in which air intrusion is caused by water emptying from a pipeline, the motion of air cavities of finite volume is essentially analogous to air pockets and also studied in the realm of gravity currents.

The study by [Zukoski (1966)] aimed to determine in a more precise manner the influence of surface tension, viscosity, and tube inclination on the propagation rate of air bubble in vertical tubes for the flow regime in which surface tension effects are important. It was determined that tube material had no influence on flow when the diameter was larger than 2 cm. Also, for Reynolds numbers greater that 200, propagation rate become substantially independent of viscous effects. The propagation rate of these bubbles increases to a maximum value as the inclination angle decreases from the vertical position to 45 degrees; a further

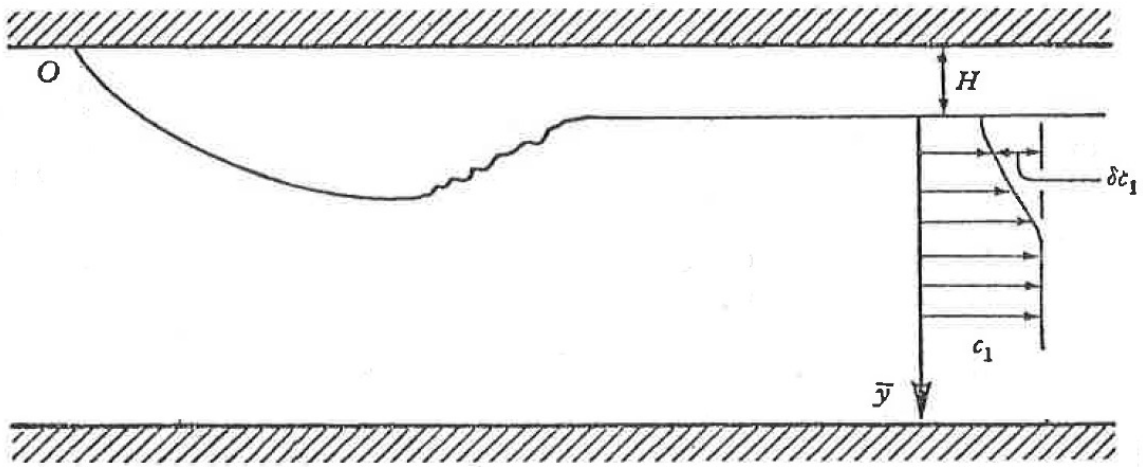


Figure 1.8: Gravity current propagation velocity adapted from [Benjamin(1968)].

reduction in the inclination angle causes the propagation rate to decrease. It was also noted that fluid occupies roughly the lower half of the tube for a horizontal inclination position and the critical speed of the air bubble is roughly $\sqrt{ga}$, where $a$ is the tube radius.

The work by [Benjamin(1968)] was one of the pioneers in establishing a that the cavity celerity scales with $\sqrt{gH}$, with g as gravitational acceleration and H the pipe characteristic dimension (e.g. diameter). Among various important observations it was found that the gravity current celerity generally decreased with its thickness. Also, this work by [Benjamin(1968)] differentiated the dissipation-free (loss-free) intrusion and the dissipative intrusion (e.g. having a trailing bore, such as Figure 1.8).

The experimental investigation by [Gardner and Crow(1970)] on the movement of large long air bubbles in stationary water in a horizontal channel of rectangular cross-section confirms the results by [Benjamin(1968)] for very deep channels, but stresses that consideration must be given to the influence of surface tension for channels as deep as 175 mm, the deepest channel investigated. This investigation also focused on the explanation of the influence of surface tension on bubble velocity. It was also noted that for deep channels, the flow is similar to that conceived by [Benjamin(1968)] except for the tip of the curved nose front near the top wall of the channel, and bubble velocity is reasonably constant with respect to distance down the channel. Surface tension was found to have a substantial effect, which is the same conclusion reached by [Zukoski (1966)] with respect to large bubbles in horizontal tubes. A limitation of these studies, similar to those previously mentioned, is the lack of ambient water flow.

The study from [Wilkinson(1982)] expanded the work by Benjamin by incorporating surface tension effects, which can markedly affect the shape and celerity of the air cavity and is more pronounced for cavities of smaller depth. However, experiments conducted in deeper ducts confirmed that surface tension becomes increasingly less significant, and the shape of the cavity approaches that of the idealized model proposed by [Benjamin(1968)]. [Wilkinson(1982)] selected frames of reference that allowed the frontal region and bore region of the cavity to be treated as steady flows, even though the flow associated with the intrusion of an air cavity into a long duct may be of an unsteady nature. Figure 1.9 shows the distinct regions of flow including: upstream region, the region of energy-conserving flow, bore, and downstream region of uniform flow.

[Baines(1991)] work followed these studies and studied an interesting air gulping flow feature observed when the pipe was set in a downward slope, in which the outlet was at a lower elevation than the inlet. This work showed that the observed celerity increased slightly with the tested slopes (up to 8 degrees), as seen in Figure 1.10, and that the celerity discrete air pockets formed after gulping also scaled with $\sqrt{gD}$. A limitation to these studies is

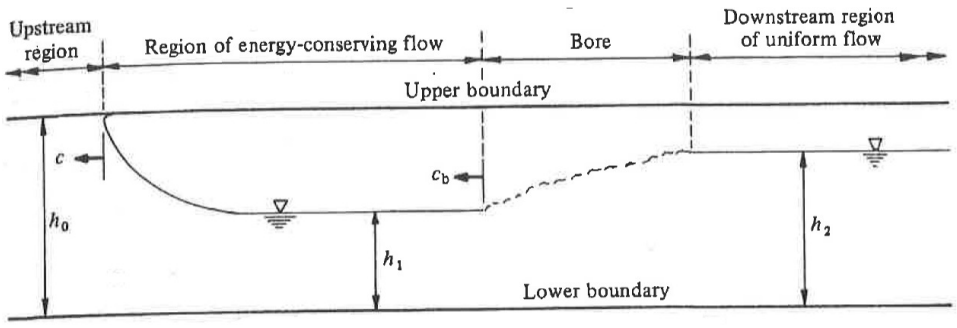


Figure 1.9: Diagram of flow schematic from [Wilkinson(1982)].

that there is no ambient water flow prior to the arrival of the air cavity; however, a general expression for the pockets celerity can be expressed as:

$$C(h) = k(h)\sqrt{gh} \tag{1.1}$$

where $C$ is the air pocket celerity, $k$ is a factor that depends on the pocket thickness, $h$ is the pocket thickness and $g$ is gravitational acceleration.

[Vasconcelos and Wright(2008)] presented an experimental and numerical work on the advance of an air cavity considering the acceleration of the water column due to varying pressure gradients. Figure 1.11 displays the advance of air intrusion observed in experimental work compared to the authors' numerical prediction. The initial advance of the air cavity is gradually halted and reverted by the water column velocity. For the largest values of $H/D$ (pressure head at the reservoir divided by the pipeline diameter), observed and predicted trajectory agree well, but for decreasing values of $H/D$ the results were not as accurate. The

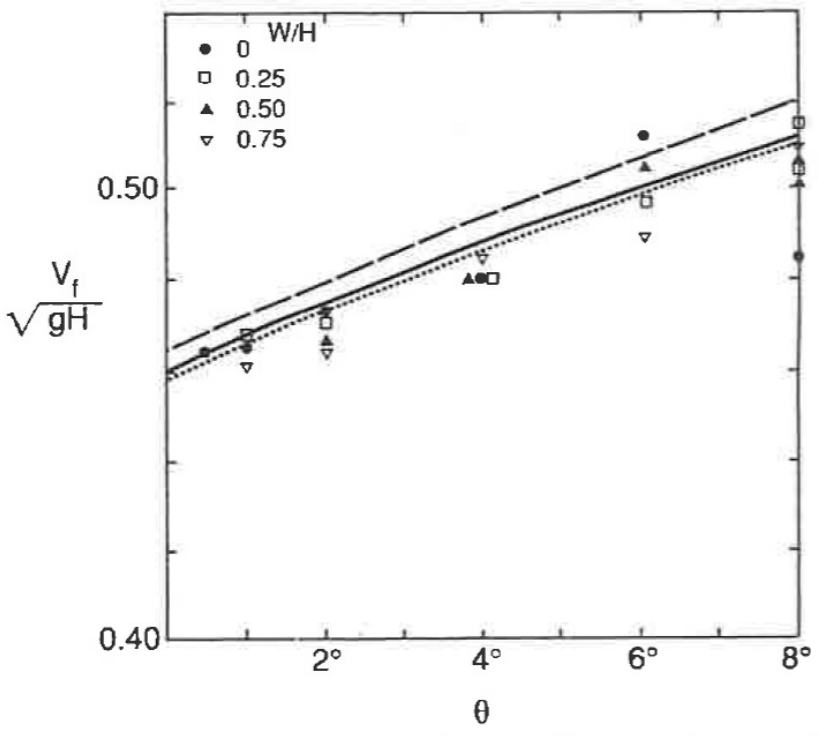


Figure 1.10: Velocity as function of channel slope from [Baines(1991)].

authors explain this discrepancy is due to the assumptions introduced into their calculations, such as assuming constant air cavity intrusion celerity. This work concluded that the loss-free intrusion analyzed by [Benjamin(1968)] does in fact adequately represent flow conditions during the initial phases of air intrusion; however, the application of this criteria to the rapid filling of an initially empty pipe does not appear to be valid. It is also important to note that this study by [Vasconcelos and Wright(2008)] has not considered such effects in discrete air pockets.

[Simpson(1997)] also presents a study on finite-volume cavities. This experimental work involved releasing a fixed volume of air into a closed horizontal tank full of water. These experiments show the clear stages of development of a gravity current of air that is released from behind a gate as it progresses above the water, as shown in Figure 1.12. Phase A shows the pocket front occupying almost exactly half the depth of the tank, and the pocket is moving at a constant speed. In phase B, a hydraulic jump (or bore) has formed at the

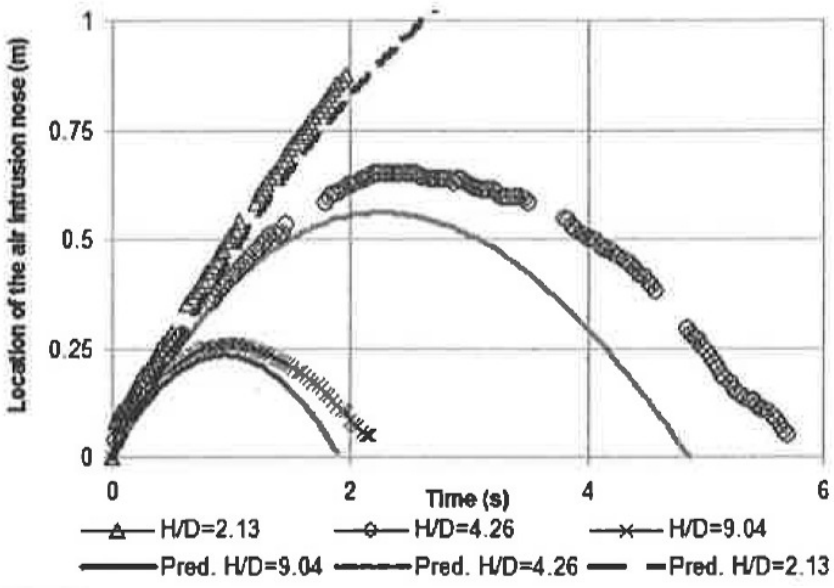


Figure 1.11: Comparison of advance of air intrusion observed in experiments with numerical prediction by [Vasconcelos and Wright(2008)].

tail of the gravity current. Finally, phase C shows that the hydraulic jump has reached the head of the gravity current, and the speed during this phase is no longer constant.

## 1.3 Hydraulic clearing of air pockets in water mains

The "hydraulic clearing" of transmission mains consists in a related application involving air pocket motion in a different context. Because of the potential issues in closed conduits, various studies have been presented to date attempting to determine a minimum value for the ambient water flow that would ensure that air pockets could be removed.

[Kalinske and Bliss(1943)] presented relevant information for a pipeline designer including the water discharge necessary to maintain air removal from any given pipe size placed at any slope based on experimental work using a 4 inch and 6 inch pipeline with varying water flow rates and pipeline slopes. It was observed that smaller air bubbles could be moved by flowing water more easily than the larger bubbles. However, these smaller bubbles gradually combine into larger bubbles, which in turn could not be moved by the water flow and as a

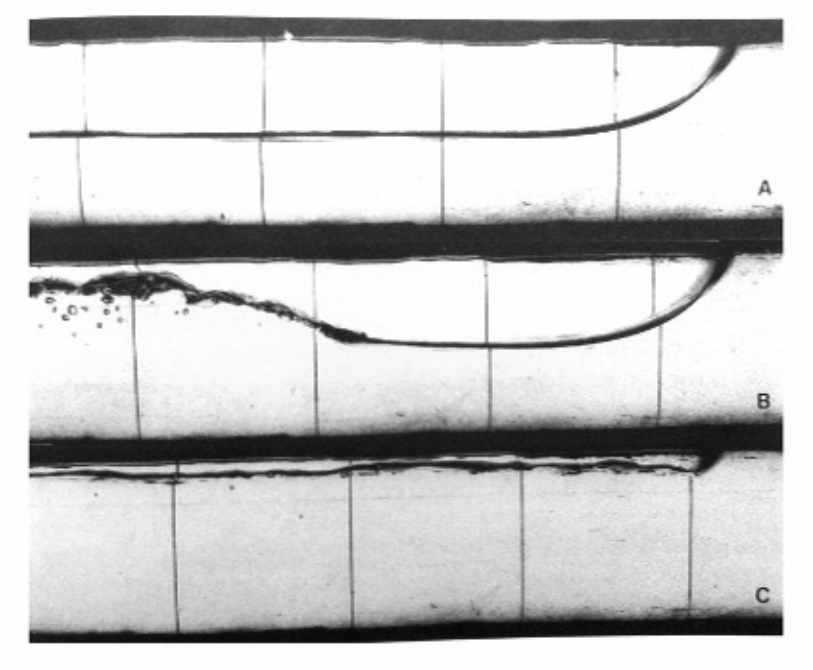


Figure 1.12: Three stages of advancing air volume released from one end of a channel of water by [Simpson(1997)].

result traveled upstream and passed through the hydraulic jump, merging with the upstream bubble.

The work by [Kalinske and Robertson(1943)] presented experimental data relating the ability of a hydraulic jump to entrain air and have it carried away by flowing water by using an apparatus with an outside diameter of 6 inches, an inside diameter of 0.49 feet, a length of 35 feet, and slopes ranging from 0.2% to 30%. It was observed that above a certain critical condition, which depends on the Froude number of the flow before the hydraulic jump, the rate of air removal from an air pocket in a pipeline will depend of the ability of the hydraulic jump which is formed within the pipe to entrain air, and an empirical relationship was presented. These pioneer studies provide useful information, but have not focused in presenting observed displacement and celerity of entrapped air pockets for various combinations of ambient flows and pipe slopes, including adverse slopes conditions.

More studies on hydraulic clearing, exemplified by works of [Falvey(1980)], [Little et al(2008)], [Pothof and Clemens(2008)] and [Pozos et al(2010b)] provide means to

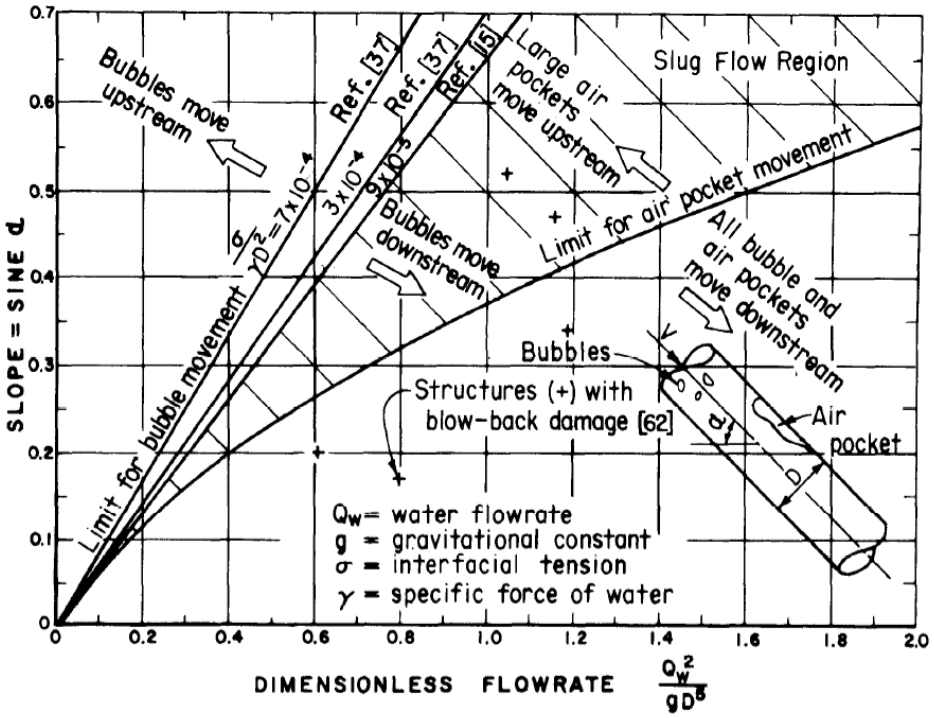


Figure 1.13: Forces acting on air pocket in closed conduit with flow [Pozos et al(2010b)].

compute the velocity magnitude at which drag forces overcomes the buoyancy forces and pockets are thus dragged downstream. Figure 1.13 presents conditions for which it is anticipated that air pockets (e.g. bubbles) will be dragged with flow (hydraulic clearing) or against flow (buoyancy) according to the pipeline geometric characteristics and background flow rate.

Figure 1.14 displays the forces that act on an entrapped air pocket presented in the work by [Pozos et al(2010b)]. The mathematical expressions for air pocket removal depend on pipeline angle and pipeline diameter, as presented in the following equation:

$$\frac{v}{\sqrt{gD}} = k\sqrt{S_0} \tag{1.2}$$

where $v$ is the critical removal velocity of water, $k$ is 1.27, $g$ is gravitational acceleration, $D$ is the pipeline diameter, and $S_0$ is the pipeline bottom slope. This equation is similar to Equation 1.1 presented in the work of [Baines(1991)] on gravity currents.

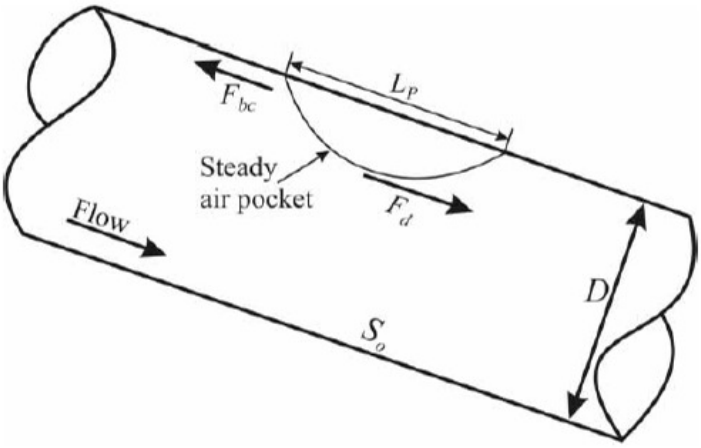


Figure 1.14: Forces acting on air pocket in closed conduit with flow [Pozos et al(2010b)].

## 1.4 Slug flows/Plug flows

Some pipeline systems are characterized by the active pumping/injection of two fluid phases (e.g. liquid/gas). These systems are usually analyzed in the realm of two-phase flows, and various types of flow regimes exist in this context. Of particular interest are slug and plug flows, which are visually similar to the air-pocket flows. It is important to note the differences between plug flow and slug flow in the context of multiphase flows, and Figure 1.15 displays the various types of flow regimes for horizontal two-phase flow. [Falvey(1980)] differentiates slug flow as having wave amplitudes that are large enough the seal the conduit, and this wave forms a frothy slug where it touches the roof of the conduit; this slug travels with a larger velocity than the average liquid velocity. Plug flow, however, occurs for increased air flow rates. These air bubbles combine with plugs of air and water alternately flowing along the top of the conduit.

[Lauchlan et al(2005)] defines plug flow as pockets or plugs that are entrapped in the main water flow, which are transported with flow along the top of the pipeline, and slug flow occurs when surface waves are large enough to seal the conduit causing the slug to travel

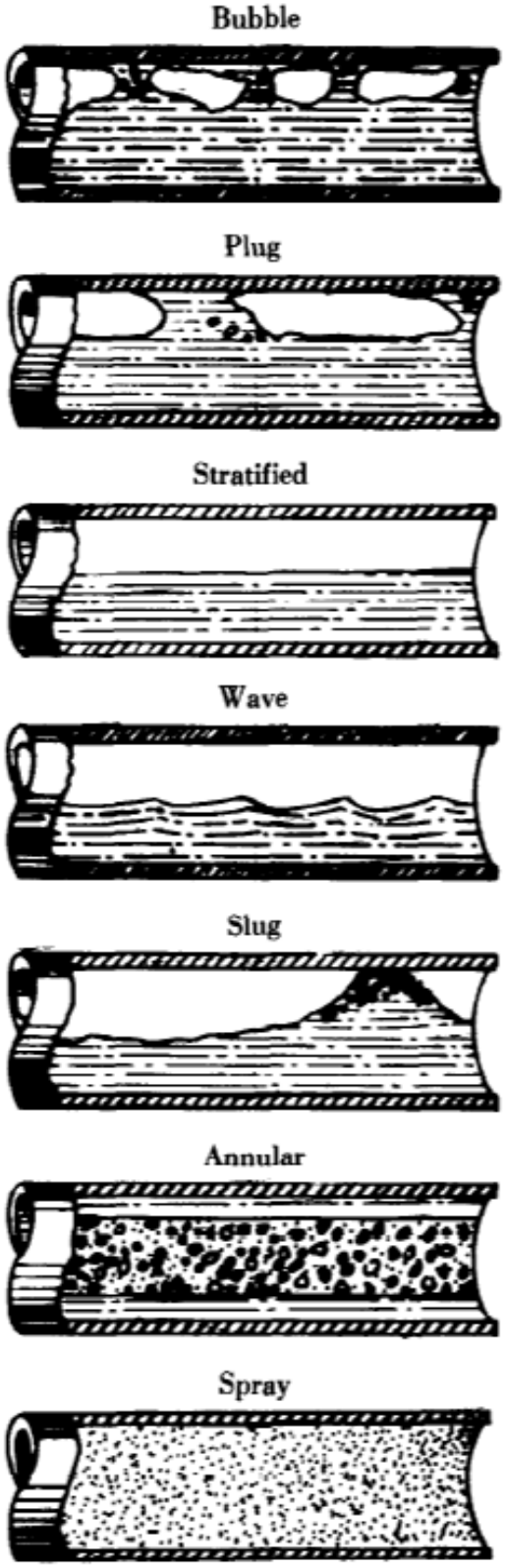


Figure 1.15: Plug and slug flow patterns as distinguished by [Falvey(1980)].

with a velocity larger than that of the liquid, which are similar to those definitions presented by [Falvey(1980)].

Two types of slugging mechanisms were identified in the work by [Lauchlan et al(2005)]: terrain induced slugging and shear induced slugging. Terrain induced slugging occurs when gas slugs form in flows in sloped terrain, and results from the accumulation of liquid phase in lower points in the pipeline, and the sudden release of gas slugs that are backed up at the upstream side of these low points. Slugs can also be generated at low elbows, dissipate at high elbows, as well as shrink and grow in length as they travel along the pipeline. Shear induced slugging occurs when hydraulic jumps promote air pocket entrainment such as Figure 1.5. The turbulent shear region contributes substantially to the air-water transfer at a hydraulic jump because its large air content and small bubble sizes resulting from large turbulent shear stress creates a very large region of air-water interface.

## 1.5 Summary of Introduction

There are many causes for air pocket formation and motion and different analysis frameworks have been developed to study such flow conditions. The frameworks proposed to study air-water flows in various contexts such as air pocket entrapment in hydraulic systems, studies on gravity currents, hydraulic clearing, and slug flow studies. However, some operational issues such as geysering, pressure surges, and flooding require deeper understanding of entrapped air pocket kinematics. This focus on operational issues and air pocket kinematics is further explored in Chapter 2.

# Chapter 2

# Literature Review

Below grade stormwater storage tunnels create a cost-effective method for relief to stormwater collection systems during intense rain events in densely urbanized areas. These storage tunnels can prevent combined sewer overflow (CSO) events as well as other related environmental issues. In most cases, these tunnel systems are very large structures, ranging in diameter sizes from 15 to 30 ft and spanning over several miles below cities. The application of these systems can be seen as early as the late 1970's in areas such as Chicago and San Francisco. Operational problems in these systems, like damaging pressure surges, led to investigations which focused in identifying the causes of these problems which have been observed when tunnel undergo rapid filling during intense rain events. Recent studies have been helpful in identifying the role that entrapped air pockets have in these flows. Evidence suggests that these entrapped air pockets have major impacts in system behavior such as pressure surge magnitude, storage capacity loss, and geysering. An improved understanding of air pocket behavior in these systems can result in the creation of better design guidelines to avoid such adverse conditions, which are sometimes present in other hydraulics systems such as water mains.

## 2.1 Issues related to air pocket entrapment

Other operational issues that have appeared in stormwater storage tunnels during intense rain events include: damaging pressure surges, manhole lid blow-off, and return of conveyed water to grade. A survey conducted by [Lautenbach and Klaver(2010)] with tunnel operators in urban areas provides an idea of the extent of these issues. Of the nine stormwater tunnel systems surveyed, seven operators indicated the occurrence of operational issues


Figure 2.1: Different urban geysering incidents: (A) Image from geyser video, reportedly recorded at Chicago, IL on 06/23/2010; (B) geyser lifting a car in Montreal, Quebec on 07/18/2011.

with varying levels of severity from displaced manholes, to structural damage and return of conveyed water to grade. One of the most extreme examples of the adverse interactions between stormwater and entrapped air is the occurrence of urban geysering, which is defined as the sudden release of a mix of conveyed water and air through ventilation shafts. Figure 2.1 presents images of recent geyser episodes recorded in urban areas resulting from intense rain events. These images suggest a variety of public health and safety hazards including the release of poor quality water to the ground surface and the flooding of major roadways. Evidence of the relationship of geysering and the rapid filling of closed conduits may be found in works by [Guo and Song(1991)], [Nielsen and Davis(2009)] and [Wright et al(2011)].

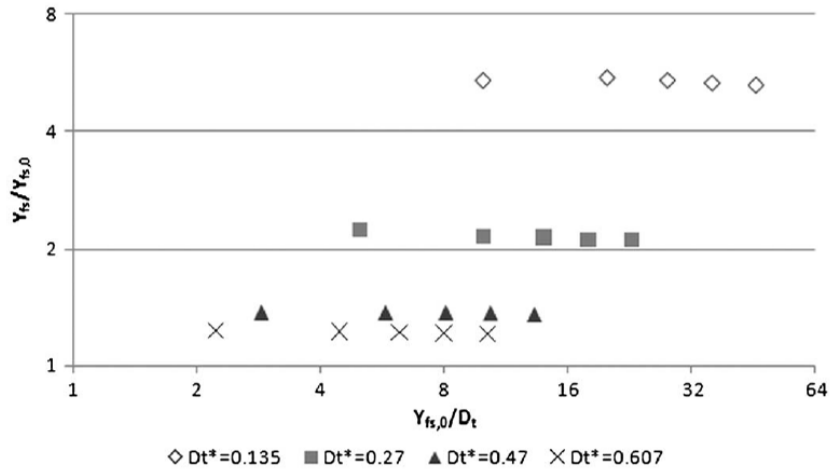


Figure 2.2: Numerical predictions for normalized free-surface level rise for differing initial free-surface levels and ventilation tower diameters [Vasconcelos and Wright(2011)].

One of the clearest adverse impacts of air pocket entrapment is the increased potential for structural damage, caused by the great compressibility of air that leads to increased surging. The pioneer study by [Martin(1976)], which was followed by [Zhou et al(2002)] among others, indicates that compressed air pressure can greatly exceed the pressure that drives the flow prior to air compression, as displayed in Figure 2.3. [Zhou et al(2002)] points that such compression may be behind an episode in which an entire manhole structure was blown off the pipe in Edmonton, Alberta. This study also separates pressure oscillations patterns in to three types of behavior: Type 1 - Negligible Water Hammer Effect, Type 2 - Mitigated Water Hammer Effect, and Type 3 - Water Hammer Dominated. These patterns were separated by observing the pressure oscillations associated with changing the size of the ventilation orifice located at the downstream end of the experimental apparatus. Figure 2.4 shows the pressure peaks associated with the most extreme of these behaviors, Type 3, which creates a great potential for structural damage.

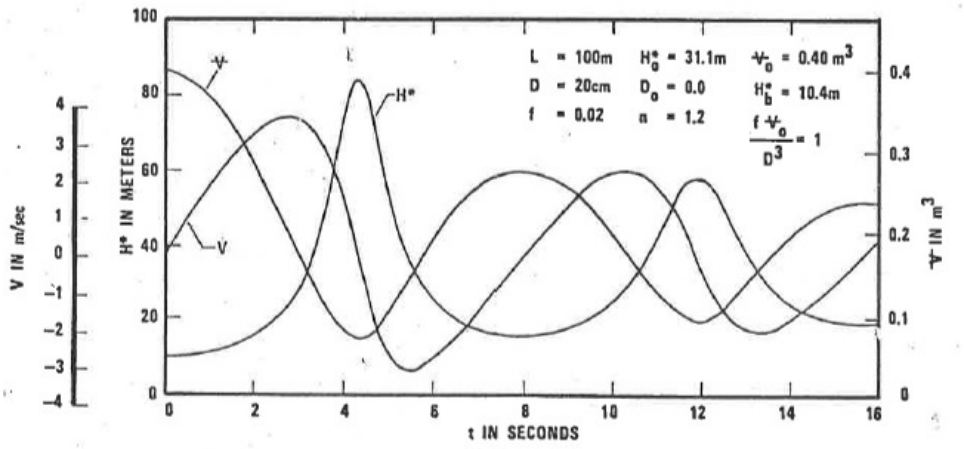


Figure 2.3: Transient air pressure, liquid velocity, and air volume [Martin(1976)].

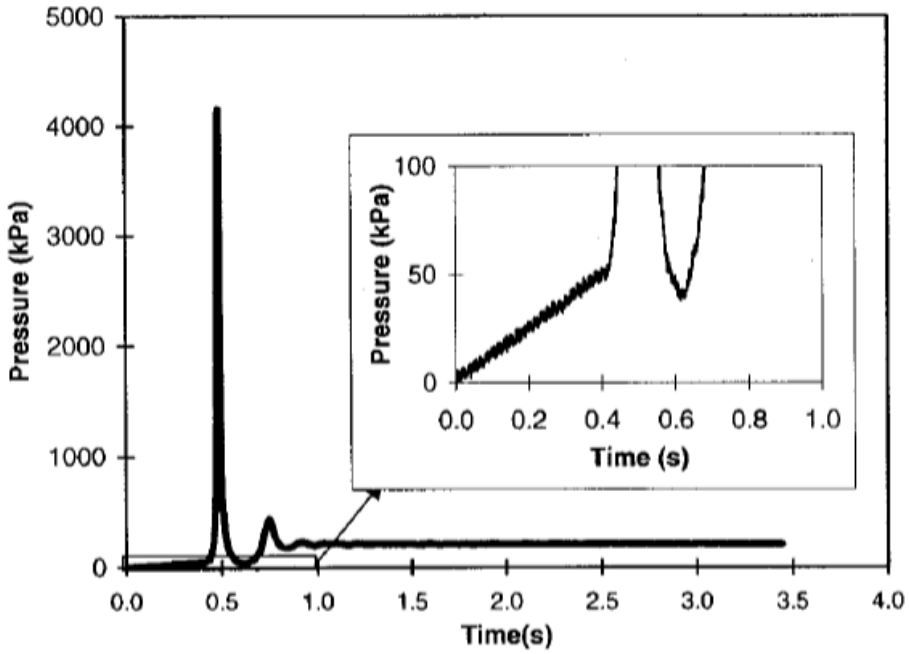


Figure 2.4: Pressure oscillation pattern for water hammer effect, Type 3 [Zhou et al(2002)].

Issues related to potential structural damage in rapid filling of closed conduits have also been explored by [Song et al(1983)], [Guo and Song(1991)], in the context of pressurization of large stormwater tunnels. Such earlier works, however, focused in a single phase framework for this medium description neglecting the influences of air phase in the problem. A more recent work by [Vasconcelos and Leite(2012)] involving air-water interaction confirms earlier findings by [Martin(1976)], but also shows that when relief is provided next to the location where air is compressed, as would be anticipated in actual tunnel geometries, the pressure rise can be significantly mitigated as presented in Figure 2.5.

Another adverse impact related to air pocket entrapment is loss of conveyance and storage capacity in closed conduits. As shown as early as [Falvey(1980)], entrapped air pockets act as flow constrictions generating additional turbulence and hence energy losses. Also, large entrapped air pockets will occupy a volume in closed conduits that would otherwise be filled with water. This is a relevant issue in the context of stormwater storage tunnels since early pressurization of these systems can lead to more frequent episodes of combined sewer overflow (CSO).

Release of entrapped air pockets can be a problematic issue as well. In the context of force mains one concern is the possibility of air slamming, defined as the waterhammer-type pressures observed at the moment when entrapped air pockets are completely evacuated through air valves. The study by [Lingireddy et al(2004)] presents a formulation to calculate such peaks in terms of the diameter of the pipeline, the diameter of the air valve and the air pocket pressure.

Another issue related to air release is geysering episodes, as sketch in Figure 2.6. The initial theoretical framework for the investigation of geysers presented by [Guo and Song(1991)] was based on inertial oscillations of the water mass within closed conduits. This single-phase approach assumed that when the hydraulic grade line (HGL) is above

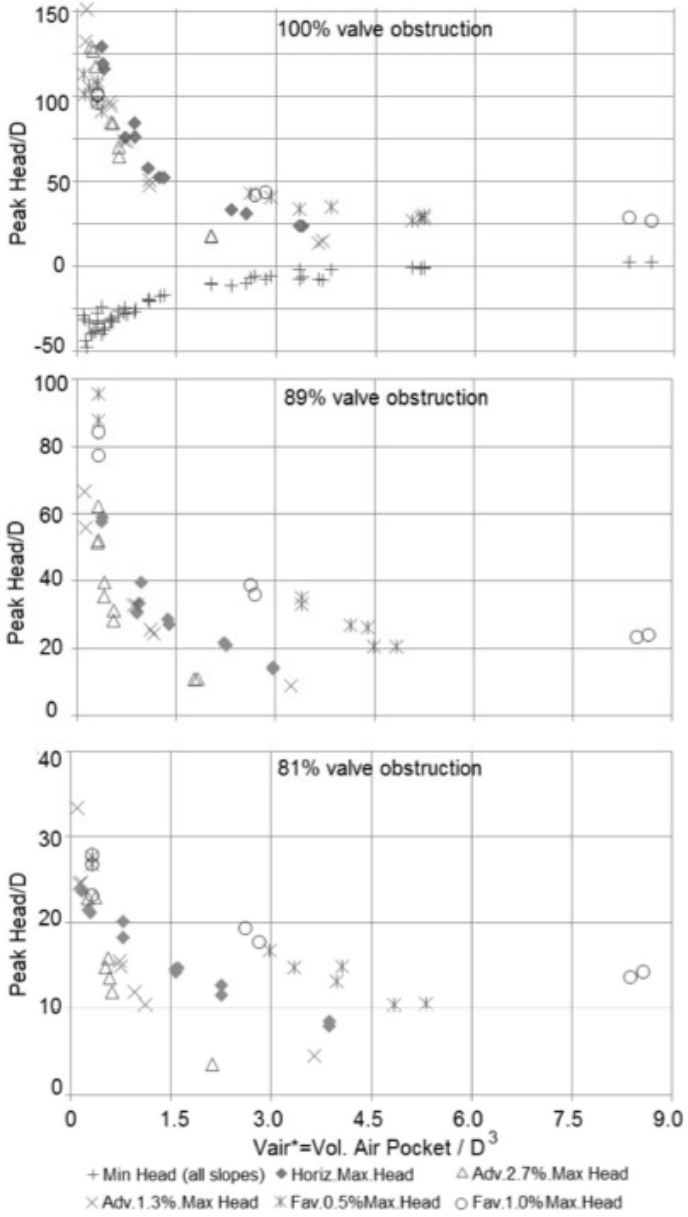


Figure 2.5: Decrease of pressure peak for various slopes, valve obstructions, and air pocket volume by [Vasconcelos and Leite(2012)].

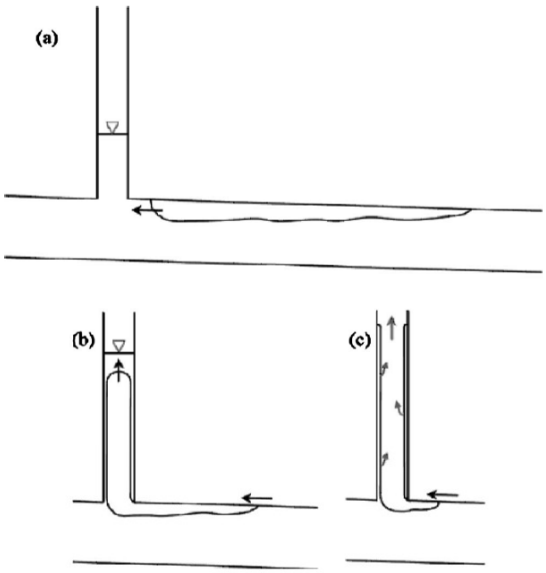


Figure 2.6: Conceptual sketch by [Wright et al(2011)] of geyser during release of large air pocket: (a) pocket migrates toward vertical shaft; (b) momentum of air pocket into shaft due to buoyancy cause rise in water level and (c) high velocity air may entrain liquid due to flooding instability.

grade geysers will occur. While this is correct, such an approach could not explain the violence and intensity of the episodes observed in penstocks [Nielsen and Davis(2009)], in physical modeling studies [Vasconcelos and Wright(2011)], and in field observations of large trunk sewers [Wright et al(2011)]. Evidence of field pressure measurements during an actual geysering episode presented by [Wright et al(2011)] show that these strong geyser episodes occurred even when the HGL was far below grade. Experimental work by [Vasconcelos and Wright(2011)] has shown that the release of large air pockets through water-filled ventilation towers may lead to geysering, and the likelihood of these events increases significantly for smaller diameter ventilation towers. Experimental results shown in Figure 2.2 indicated that air pocket release through water filled shafts of smaller diameters increased geyser likelihood.

While these previous investigations are very relevant, a key problem that is less understood is the kinematics of these entrapped air pockets. The ability of describing the motion of entrapped pockets would be useful as it would help to assess the effectiveness of air pocket removal in transmission mains. It would also assess the likelihood of uncontrolled air release through ventilation shafts in stormwater systems.

## 2.2 Experimental investigations on air pocket kinematics

The experimental investigation presented by [Aimable and Zech(2003)] depicts the results on the formation of an air cavity and intermittent flows in a small-scale laboratory sewer model ($D = 0.144$ m and $S = 1.5\%$ to $1.45\%$) that is similar to a reach of a real-world sewer system. The authors intended to mimic shear force mechanisms for pocket generation such as in the work by [Li and McCorquodale(1999)]. This work concludes that the behavior of an air cavity is influenced by discharges and the rate of variation in the downstream boundary of the system. An important observation is that the velocities of the two ends of a mixed flow section are rather different during the air release process.

[Perron et al.(2006)] presented a work investigating the influence of surface inclination and bubble volume on the terminal velocity of relatively large air bubbles with volumes ranging from 0.3 to 0.9 cubic centimeters and a surface inclination varying from 2 to 10 degrees. An important note is that the apparatus used in these experiments was not a pipe, but an inclined plate as seen in Figure 2.7. The authors observed that the terminal velocity of a given bubble volume increased with inclination angle, and this increase was important for both low bubble volumes and low inclination angles. Both surface tension and viscous forces played a role for bubble of small volume at low inclination angles. For higher bubble volumes, the increase in terminal velocity followed a more linear relationship. These studies have a limitation in their ability to evaluate effects such as air pocket spreading observed in horizontal slopes.

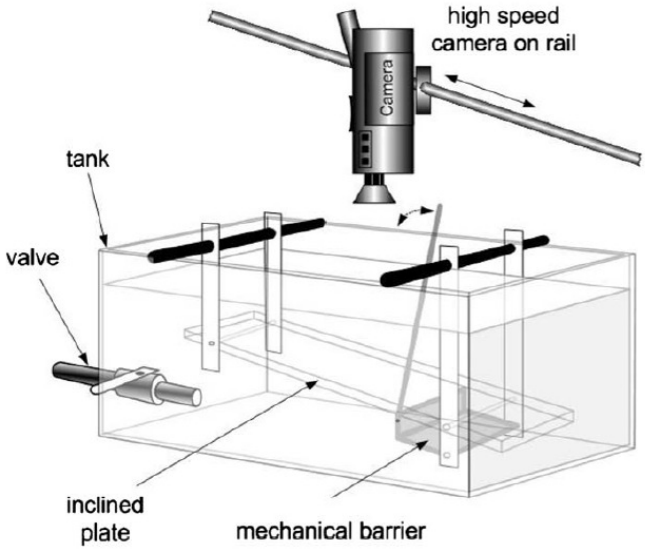


Figure 2.7: Schematic of experimental apparatus used by [Perron et al.(2006)].

[Glauser and Wickenhauser(2009)] provided an experimental study on the dynamics of an air cavity advancing in a pressurized pipe. The focus was on the shape and movement of single air bubbles in continuous air-water flow with the intention to determine the bubble volume that represents the stagnation velocity based on a balance of buoyancy and drag forces. It was noted that in favorably sloped pipes, volumes larger than this critical volume move against this flow due to buoyancy and volumes smaller than this critical volume would be dragged by the flow against buoyancy. Similarly to studies in hydraulic clearing of water mains, it was determined that pipeline slope, background water velocity, and bubble volume controls the observed pocket celerity. This investigation involved the use of slopes ranging from 1.7% to 8.7%, thus always involving conditions where buoyancy forces opposed flow drag forces.

## 2.3 Numerical investigations on air pocket kinematics

Numerical studies have been presented in attempting to describe patterns related to the motion of entrapped air pockets in closed conduit flow. The majority of these studies are in the realm of multi-phase flow applications, and exemplified by the works of [Barnea and Taitel(1993)], [DeHenau and Raithby(1995)] and [Issa and Kempf(2003)]. In these applications there is a continuous injection of gas and liquid in closed conduits, and the mechanisms for pocket formation are diverse (e.g. terrain induced slugging) from the ones that are generally observed in water, wastewater and stormwater systems. [Issa and Kempf(2003)] presented the following equations to describe one-dimensional stratified and slug flow, which are solved for the conservation of mass and momentum for both gas and liquid phases:

$$\frac{\partial(\rho_g \alpha_g)}{\partial t} + \frac{\partial(\rho_g \alpha_g \mu_g)}{\partial x} = -\dot{m}_b \tag{2.1}$$

$$\frac{\partial(\rho_l \alpha_l)}{\partial t} + \frac{\partial(\rho_l \alpha_l \mu_l)}{\partial x} = \dot{m}_b \tag{2.2}$$

$$\frac{\partial(\rho_g \alpha_g \mu_g)}{\partial t} + \frac{\partial(\rho_g \alpha_g \mu_g^2)}{\partial x} = -\alpha_g \frac{\partial p}{\partial x} + \rho_g \alpha_g g \sin\beta + F_{gw} + F_i \tag{2.3}$$

$$\frac{\partial(\rho_l \alpha_l \mu_l)}{\partial t} + \frac{\partial(\rho_l \alpha_l \mu_l^2)}{\partial x} = -\alpha_l \frac{\partial p}{\partial x} - \rho_l \alpha_l g \frac{\partial h}{\partial x} \cos\beta + \rho_l \alpha_l g \sin\beta + F_{lw} - F_i \tag{2.4}$$

where

$$\alpha_g + \alpha_l = 1 \tag{2.5}$$

The subscripts $g$, $l$, and $i$ refer to the gas phase, liquid phase, and interface, respectively. Also, $x$ is the axial coordinate, $\rho$ is the density, $\alpha$ is the phase fraction, $\mu$ is the velocity,

$\dot{m}_b$ is the mass transfer per unit volume between the phases, $p$ is the interface (and gas) pressure, $\beta$ is the pipeline angle, $h$ is the height of the liquid surface (assumed to be flat) above the pipeline bottom, and $g$ is the gravitational acceleration. It is assumed that the liquid phase is incompressible, while the gas phase is considered compressible obeying the ideal gas law, and the flow is also assumed to be isothermal for simplicity. The second term on the right-hand side of equation 2.3 relates to the hydrostatic pressure in the liquid phase and is specific to the stratified and slug flow regimes. The $F$ terms represent the frictional forces per unit volume between each phase and the pipeline wall, and between the phases themselves (at the interface).

The study by [Li and McCorquodale(1999)] present mathematical framework for the simulation of flow regime transition (also referred to as mixed flows) using lumped inertia analysis and the ideal gas law, and consider the mechanism for air pocket formation based on shear flow instabilities presented by [Hamam and McCorquodale(1982)]. Figure 2.8 displays the stages in transition of free-surface to pressurized flow by [Li and McCorquodale(1999)]. In the formulation the location of the air-water interface is calculated explicitly, providing then means to compute the advance of an entrapped pocket. Yet, the velocity of the air bubble, rather than be calculated by the model, appears as a calibration parameter in the simulations.

More recently [Trindade and Vasconcelos(2013)] presented a study that included a numerical framework to simulate pipeline priming operations considering the possibility of air pressurization using the Two-component Pressure Approach (TPA) following the work by [Vasconcelos and Wright(2009)]. With regards to air pressurization, this work included the possibility of air pressure variation along the length of the air pocket, which was computed using the isothermal Euler equations. The model updates the air-water interface using a source term for the Euler equations presented in [Toro(2009)]. The equations applied by the TPA model, exemplified in the work of [Trindade and Vasconcelos(2013)], modify the

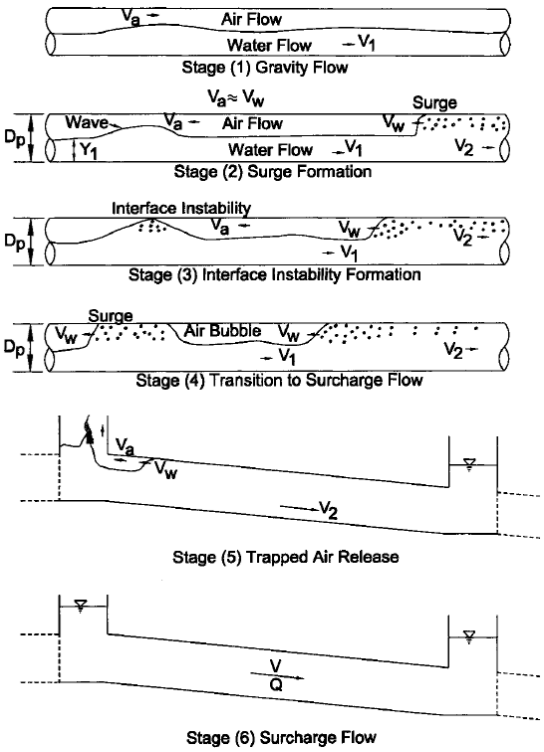


Figure 2.8: Stages of flow transition by [Li and McCorquodale(1999)].

Saint-Venant equations enabling them to simulate pressurized and free-surface flow regimes and are shown below:

$$\frac{\partial \mathbf{U}}{\partial t} + \frac{\partial \mathbf{F}(\mathbf{U})}{\partial x} = \mathbf{S}(\mathbf{U}) \tag{2.6}$$

where

$$\mathbf{U} = \begin{bmatrix} A \\ Q \end{bmatrix} \qquad \mathbf{F}(\mathbf{U}) = \begin{bmatrix} Q \\ \dfrac{(Q)^2}{A} + gA(h_c + h_s) + gA_{pipe}h_{air} \end{bmatrix} \qquad \mathbf{S}(\mathbf{U}) = \begin{bmatrix} 0 \\ gA(S_0 - S_f) \end{bmatrix} \tag{2.7}$$

$$h_{air} = \begin{cases} = 0 & \rightarrow \text{Free-surface flow without entrapped air pocket or pressurized flow} \\ \neq 0 & \rightarrow \text{Free-surface flow with entrapped air pocket} \end{cases} \tag{2.8}$$

$$h_s = \begin{cases} 0 & \rightarrow \text{Free-surface flow} \\ \dfrac{a^2}{g}\dfrac{(A - A_{pipe})}{A_{pipe}} & \rightarrow \text{Pressurized flow} \end{cases} \tag{2.9}$$

$$h_c = \begin{cases} \dfrac{D}{3}\dfrac{3\sin\theta - \sin^3\theta - 3\theta\cos\theta}{2\theta - \sin 2\theta} & \rightarrow \text{Free-surface flow} \\ \text{where } \theta = \pi - \arccos\left[(y - D/2)(D/2)\right] & \\ \dfrac{D}{2} & \rightarrow \text{Pressurized flow} \end{cases} \tag{2.10}$$

where $\mathbf{U} = [A, Q]^T$ is conserved variables vector, $A$ is the cross-sectional area of flow, $Q$ is the flow rate, $\mathbf{F}(\mathbf{U})$ is the flux of conserved variables vector, $g$ is gravitational acceleration, $h_c$ is the distance between the free surface and the centroid of the flow cross-section (limited to $\frac{D}{2}$), $h_s$ is the surcharge head, $h_{air}$ is the extra head due to entrapped air pocket pressurization, $\theta$ is the angle formed by free surface flow width and the pipe centerline, $D$ is the pipeline diameter, $A_{pipe}$ is the pipeline cross-sectional area, and $a$ is the celerity of acoustic waves in pressurized flow. Two modeling approaches were used for the air phase description. The first one applies the isothermal Euler equation, whereas the second alternative assumes uniform air pressurization (UAPH model).

Figure 2.9 indicates the model accurately predicted the trajectory of air-water interface including complex flow interactions, including interface breakdown of the pressurization interface. A limitation of that model is that the only mechanism that is accounted for the motion of the air-water interface is the displacement of air that is caused by the advancing water interface during the priming event. Also, it was assumed that one of the boundaries

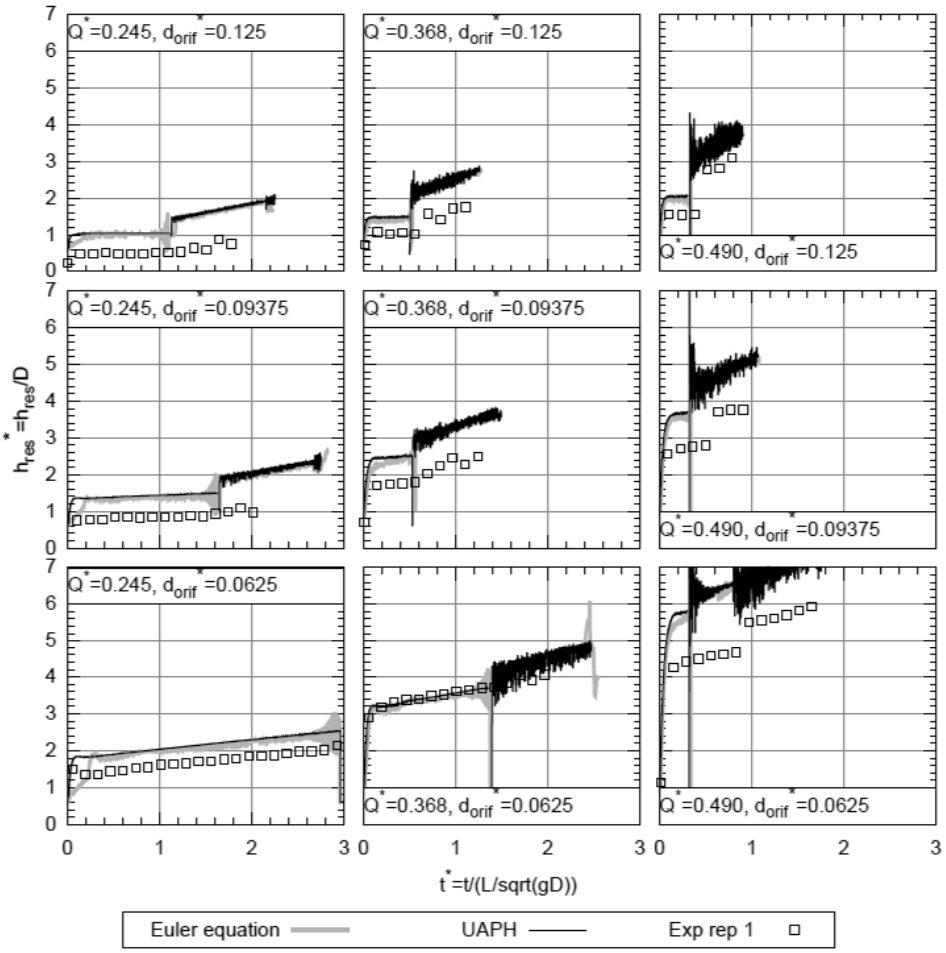


Figure 2.9: Measured and predicted pressures at pipe crown for $x^*$=0.39, $d_{orif}$¡0.5, and slope 1% by [Trindade and Vasconcelos(2013)].

of the air pocket was fixed at the air release valve. Another difficulty for the simulation of entrapped pockets motion is that one dimensional models generally are constructed with the hypothesis of hydrostatic pressure distribution at the flow cross sections, which will not hold at the strongly curved air-water interfaces.

# Chapter 3

## Knowledge Gap and Objectives

Although the previous studies in areas such as air pocket velocity, clearing velocity, air pocket movement and air pressure estimation have led to significant developments in the area of air-water interaction in stormwater storage tunnels, there still remains a significant knowledge gap in this field. This knowledge gap may be summarized as follows:

- Gravity current investigations, such as those by [Benjamin(1968)], [Wilkinson(1982)], [Baines(1991)], [Zukoski (1966)], and [Gardner and Crow(1970)], describe motion of air-water interfaces but disregard effects of ambient water flow.

- Air cavity intrusion into unsteady flow considered by [Vasconcelos and Wright(2008)] does not consider the case of discrete air pockets.

- Hydraulic clearing studies, exemplified in the works of [Falvey(1980)], [Little et al(2008)], [Pothof and Clemens(2008)], [Pozos et al(2010b)], etc., have not focused on the kinematics of entrapped air pockets for varying conditions of ambient flow and pipeline slope.

- Studies focused on the motion of entrapped air pockets presented by [Aimable and Zech(2003)], [Perron et al.(2006)], and [Glauser and Wickenhauser(2009)] do not provide information on air pocket spreading in horizontally sloped pipelines or images when drag and buoyancy forces are added.

A better understanding of the kinematics of these air pockets in stormwater storage tunnels is needed so that better design guidelines can be proposed to avoid adverse conditions such as pressure surges, storage capacity loss, and geysering.

The main objective of this research is to explore a link between ambient flow velocity, pipeline slope and the celerity of entrapped air pockets of various volumes. This research explores these links through previously unexplored processes that include the following:

- Study the motion of entrapped air pockets with and without ambient flow velocity.
- Physically contain a discrete entrapped air pocket at a determined location with the use of knife-gate valves while allowing background flow to circulate.
- Focus on the kinematics of entrapped air pockets for varying adverse, horizontal, and favorable pipeline slopes as well as varying conditions of ambient flow.
- Explore entrapped air pocket motion when drag and buoyancy forces are opposing one another in very shallow and horizontal pipes.

This work presents experimental results from a physical model investigation on the kinematics of entrapped air pockets in pressurized water flows under shallow slopes. Discussion of the experimental results is presented along with conclusions and recommendations for future work.

# Chapter 4

# Methodology

## 4.1 General description and rationale of the experiments

The apparatus for this experimental investigation was created from 102 mm clear PVC pipe supported by a steel frame which could have its slope adjusted manually and is presented schematically in Figure 4.1. Two reservoirs of approximately equal volume, 0.63 $m^3$, were secured upstream and downstream of the PVC pipeline. The upstream reservoir was connected to the pipeline by a control valve which could stop flow if necessary. Water was allowed to flow steadily underneath partially opened knife gate valves into the downstream reservoir, ensuring pressurized flow regime in the pipeline. A clear, acrylic cylinder was attached to the bottom of the PVC pipeline and connected to it through a ball valve in order to allow for air introduction into the system. Another valve was placed on this acrylic cylinder allowing atmospheric air into it.

The experimental protocol was developed with the idea of allowing an air pocket of known volume into a closed conduit system while still allowing a known background flow to circulate. It was determined that once the air pocket was injected into the system, a new steady-state needed to be reached due to the extra head loss throughout the system caused by the addition of this pocket. A ruler was attached along the length of the pipeline in order to track the location of the air pocket front edge during experiments.

Figure 4.1 presents a schematic of the apparatus used in the experimental procedure for horizontal and adverse (pipeline downstream end at a higher elevation than upstream end) pipeline slopes. These experiments were performed with a variable slope, clear PVC pipeline supplied upstream by a fixed head reservoir with a throttled discharge downstream to ensure pressurized flow throughout the pipeline. The pipeline has a length $L = 11.1$ m

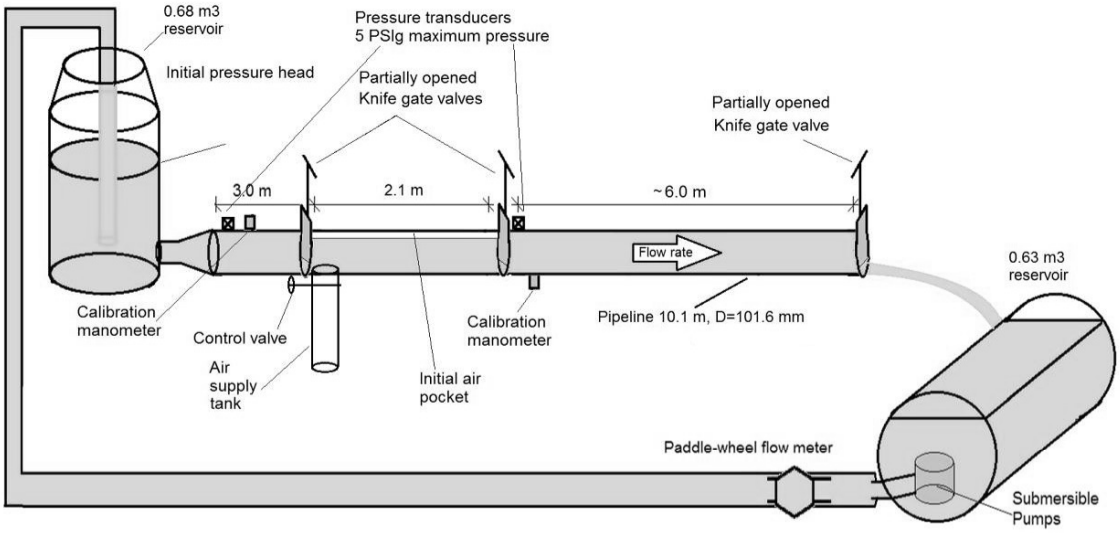


Figure 4.1: Sketch of apparatus used in horizontal and adverse pipeline slope experiments.

and a diameter $D = 101.6$ mm. The upstream supply reservoir is attached to the pipeline by a 50 mm diameter ball valve. Two knife gate valves with the same diameter as that of the pipeline were positioned 3 m downstream of the upstream supply reservoir with a 2.1 m separation for adverse and horizontal sloped conditions.

For favorable (pipeline downstream end at a lower elevation than upstream end) slopes, upstream and downstream reaches have lengths of 6 m and 3 m respectively, as shown in Figure 4.2. The apparatus was adjusted to allow video cameras to have a longer viewing range of air pocket pocket motion propagating upstream due to buoyancy forces.

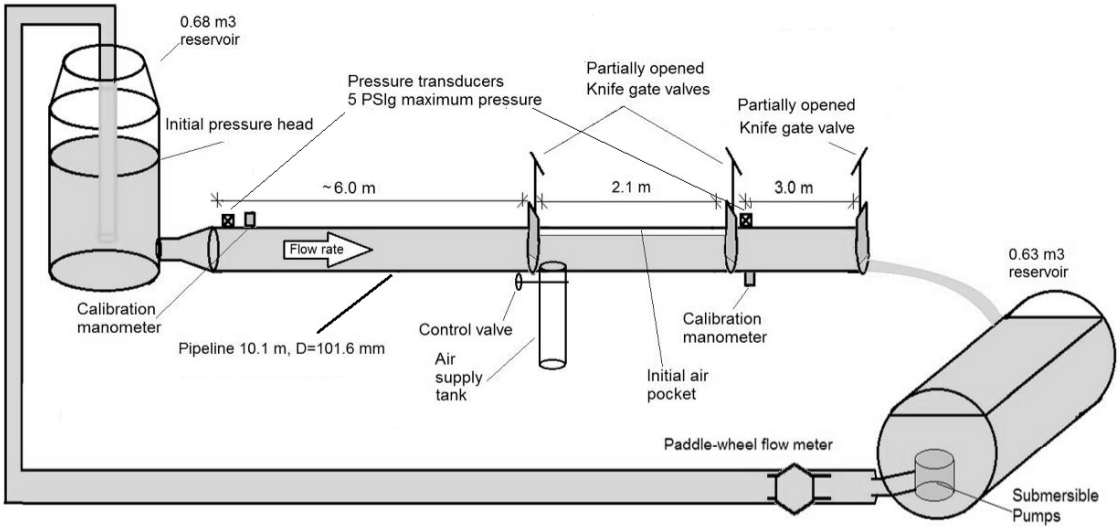


Figure 4.2: Sketch of apparatus used in favorable pipeline slope experiments. Changes were only in the location of internal knife gate valves.

Pre-determined volumes of air at atmospheric pressure were injected into the region between the two knife gate valves forming an air pocket. These partially closed knife gate valves prevented the motion of the air pockets while still allowing flow underneath. The specific air volumes were determined by back-calculating the amount of water that filled the graduated acrylic tank located below the clear PVC pipeline once the valve connecting these pieces was opened. A valve connecting the graduated acrylic tank to the atmosphere ensured that the air was at atmospheric pressure when injected into the water-filled pipeline.

The measurement devices used in the experimental procedure include:

- Up to four high definition camcorders (1080 pixels, 30 FPS), providing a total view of 7.0 m upstream and downstream of the intermediate knife gate valves;

- Two piezoresistive pressure transducers, MEGGIT Endevco 8510B-5 (±1% accuracy), located at the upstream end ($L^1 = X/L = 0.0$) and at approximately 50% of the pipeline length ($L^1 = 0.5$), recording with a frequency of 100 Hz for each channel;
- National Instruments data acquisition board NI-USB 6210 with SignalExpress logging software;
- EXTECH digital manometers (±0.3% accuracy) located at both ends of the apparatus and at 50% of the pipeline length ($L^1 = 0.5$); and
- Cole-Palmer paddle wheel flow meter (±1% accuracy) to gage ambient flow rate.

## 4.2 Experimental program

The results presented in this paper include 99 differing conditions. Seven slopes have been tested: horizontal slope, 0.5%, 1.0%, and 2.0% adverse slope(downstream end at higher elevation than inlet) and 0.5%, 1.0%, and 2.0% favorable slope (downstream end at lower elevation than inlet). For each of these slopes, three different flow rates ranging from 1.4 L/s to 4.0 L/s and up to four air pocket volumes were tested. These pocket volumes ranged between 1.3 L and 4.3 L for horizontal slopes and between 0.5 L and 4.0 L for adverse and favorable slopes. It is important to note that each case was repeated at least once in order to ensure that data was consistent. Table 4.1 presents a summary of the parameters tested in this investigation.

Table 4.1: Experimental variables considered with respective tested ranges

| Experimental variable | Range |
|---|---|
| Flow rate (normalized by $Q/\sqrt{gD^5}$) | Three values ranging from $Q^*$=0 up to 0.388 |
| Pipeline slope | Horizontal slope<br>0.5%, 1.0%, and 2.0% adverse slopes<br>0.5%, 1.0%, and 2.0% favorable slopes |
| Air pocket volume (normalized by $D^3$) | Horizontal: up to 4 values in the range $Vol^*$=1.2-4.1<br>Adverse: up to 4 values in the range $Vol^*$=0.48-3.8<br>Favorable: up to 4 values in the range $Vol^*$=0.48-3.8 |

Conditions that merited testing included those that represented a wide range of air pocket volumes, pipeline slopes, and background flow rates that stormwater storage tunnels could encounter during rapid filling after an intense rain event. Air pocket volume was determined by back-calculating the amount of water that flowed from the PVC pipeline into the acrylic cylinder when the control valve was opened to inject air.

The experimental procedure was performed as follows:

1. Set the selected slope for the pipeline apparatus;

2. Create steady flow conditions in the PVC pipeline by turning on submersible pumps at desired flow rate and opening the intermediate knife gate valves to desired opening percentage;

3. Inject air volume at atmospheric pressure by opening the valve connecting the graduated acrylic cylinder and the water filled PVC pipeline;

4. Allow system to achieve a new steady state condition due to the increase in energy losses created by the addition of air into the system;

5. Initiate pressure measurements and collect readings on calibration manometers;

6. Open the intermediate knife gate valves simultaneously and rapidly ($t < 0.6\,s$) to allow sudden release of air pocket;

7. Record motion and spreading of the air pocket(s) with camcorders until moving outside field of view; and

8. Close valves and stop submersible pumps after considerable time and make final readings on the calibration manometers.

It was noted visually that a pronounced drag created by larger flow rates caused bits of some air pockets to be dragged underneath the knife gate valves intended to keep the pocket in place as a whole until the start of the experiment. In order to keep this phenomenon

from happening, certain runs with larger air pocket volumes and larger flow rates were not performed. Along with the flow rates and air pockets volumes mentioned above, experiments were run to study the thinning of the air pocket when a single knife gate valve was opened with no background flow.

### 4.3 Data analysis

Data processing was completed by watching the video recordings of each experimental run frame by frame. The time that the pocket front reached every one foot marker on the scale attached to the pipeline apparatus was recorded. Using these time and pocket front location values, the trajectory was plotted for each experimental run. The celerity, $C$, and relative celerity, $C - v_{flow}$, values were also plotted for analysis. Piezoresistive pressure transducer data was converted into useful information (e.g. pressure oscillations) by using the linear relationship between force/pressure, strain, and return voltage gaged at the transducer membrane. Using the calibration manometers, this linear relationship was used to predict the varying pressures throughout the system during experimental runs based on the return voltage recorded by the transducers.

### 4.4 Comparison with numerical model

Results from a numerical model based on internal gravity current modeling theory, developed by [Hatcher et al(2013)], were compared to the horizontal (no slope) results acquired during the experimental investigation. This model utilizes an integral model approach as well as a relationship between the gravity current thickness (in this case, air pocket thickness) and its propagation speed to update the location of the leading edge of the pocket. This model accounts for surface tension using the approach outlined in [Wilkinson(1982)]. The effects of ambient crossflows are incorporated into this integral model using the front condition provided in [Hallworth et al(1998)]. For the following integral model formulation, this expression has been adapted to circular cross-sections:

$$u_f = \frac{dx_f}{dt} = Fr\sqrt{gD} + U \tag{4.1}$$

where $x_f$ is the distance traveled by the respective cavity front, $Fr$ is the local Froude number at the upstream and/or downstream air pocket front, $D$ is the pipe diameter and $U$ is the background flow velocity.

Two separate integral models, $M1$ and $M2$, that differ in front condition selection were analyzed. These models account for buoyancy, drag, background flows, and surface tension ($M1$). Further model details are not presented here for brevity.

# Chapter 5

# Results and Discussion

As stated earlier, a main research objective for this investigation was to further explore a link between ambient flow velocity, pipeline slope and the celerity of entrapped air pockets of various volumes, including effects of air pocket spreading. The following sections present the results of this experimental investigation, first for cases with no ambient flow and then for cases with ambient flow. The small discrepancies in air pocket volumes for cases involving horizontal slope and favorable/adverse slopes does not affect the overall analysis presented below.

## 5.1 Air pocket spreading in horizontal slope

Figure 5.1 presents the trajectories and celerity values of the air pocket front for four different air pocket volumes for horizontal slopes without ambient flow. All velocity results (celerity, relative celerity) values on figures are normalized by $\sqrt{gD} \approx 1.0$ m/s; trajectory coordinates are normalized by the original pocket length; and time is normalized by $\sqrt{D/g} \approx 0.102$ s. These results show a slightly curved trajectory of the air pocket leading edge for all the tested volumes. This curvature indicates a reduction in the leading edge celerity, caused by the air pocket spreading and reducing of the air pocket thickness consistent to results by [Benjamin(1968)]. The slope of the air pocket's leading edge trajectory decreased for larger air pocket volumes, indicating an increase in celerity, an expected result. It can be noticed that the trajectory of the back-propagating front is symmetrical to the forward propagating front in the absence of flow in the pipe, also as anticipated.

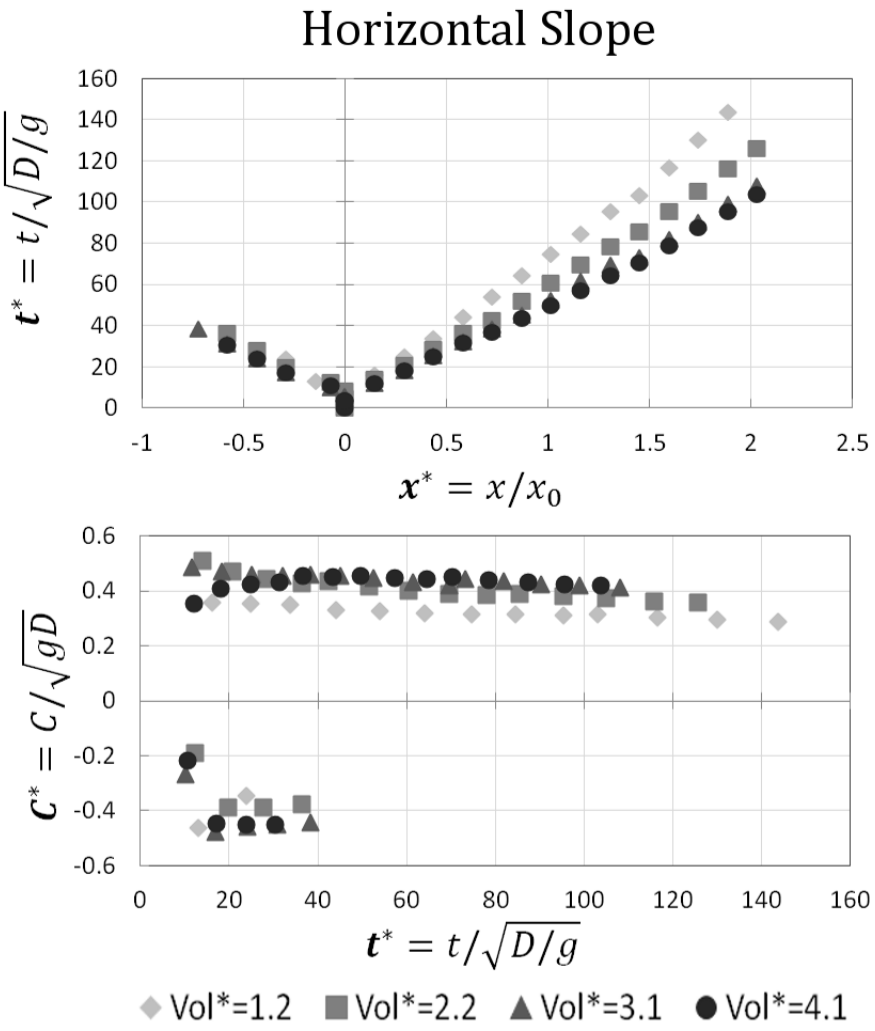


Figure 5.1: Trajectory of the air pocket leading edge and observed celerity for horizontal slope and various air pocket volumes, no ambient flow. Negative coordinates indicate pockets are propagating toward upstream.

Results are significantly affected by the presence of ambient flows. Figure 5.2 presents the trajectories for the cases with air pocket volumes of $Vol^*$=1.2 and $Vol^*$=2.2 and horizontal slope for various ambient flows. Celerity values $C^*=C/\sqrt{gD}$ are complemented by celerity values relative to the ambient flow ($C$ - $v_{flow}/\sqrt{gD}$). The symmetry between the two air pocket fronts previously observed for horizontal case is no longer observed due to drag forces caused by the introduction of ambient flow. The results in Figure 5.2 indicate that larger flow rates result in an increase in the celerity of the forward moving air pocket front, and that this gain in velocity is proportional to the ambient flow velocity. Results also indicate that in the initial stages following the pocket release there is an increase in the celerity that is generally over by time $t^* \approx 2$. The previously observed air pocket front spreading effect in the horizontal slope and no ambient flow, which led to decreasing celerity values, is not observed is when there is ambient flows. Results in Figure 5.2 support the assumption that for horizontal pipes the pocket celerity in ambient flow conditions can be estimated as the summation of its value in quiescent conditions plus the ambient flow velocity; however, this estimation is only valid after a certain time where the pocket accelerates from zero to a steady velocity.

An interesting result is that is even for the smallest tested ambient flow, the backward propagating air pocket leading edge is eventually sheared and no longer observed for values of $X^1 < 0.3$ and $t^* \approx 1$. Also, it is important to note that the $v^*_{flow}$ from ambient flow was smaller than the initial $C^*$ of the backward moving air pocket. This indicates that in the absence of buoyancy forces the propagation of discrete air pockets against an ambient flow is short lived. Figure 5.3 presents seven snapshots of the pocket propagation with 1 second time lapse between the images, for a condition corresponding to a pocket with $Vol^*$=4.1, flow rate $Q^*$=0.27, flow velocity $v^*_{flow}$=0.34, and $C^*(initial) \approx 0.68$. Air-water interfaces in the figure are artificially enhanced for clarity. The initial shape of the front resembles a typical, dissipative gravity current with a curved nose with a trailing a hydraulic jump, as described in [Benjamin(1968)]. As the front moved upstream, the trailing hydraulic jump entrained

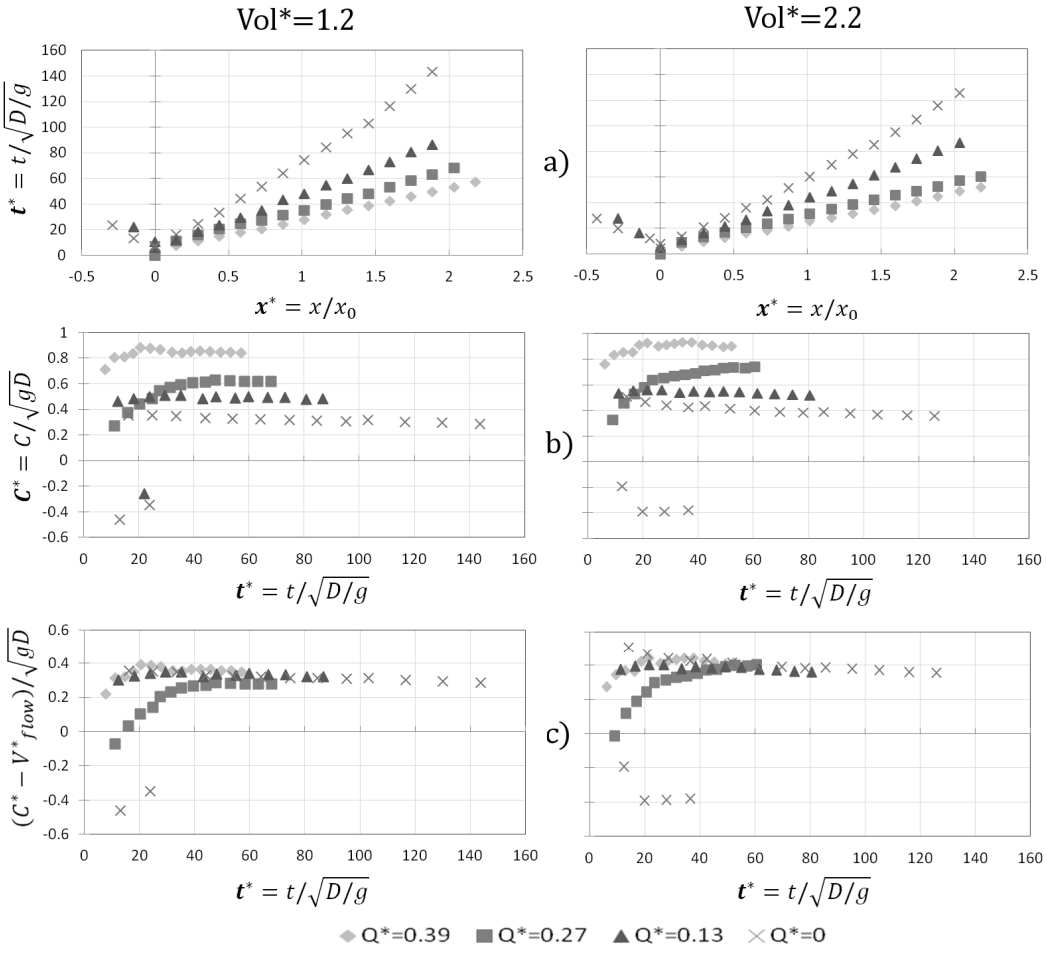


Figure 5.2: Trajectory of the air pocket leading edge, observed celerity and relative celerity for conditions with horizontal slope, ambient flow, and $Vol*$=1.2 and $Vol*$=2.2.

air at the leading edge of the pocket, and these air bubbles were carried with the ambient flow flow. The pocket volume thus decreased over time and within 7-8 seconds it effectively vanished. In the process, the observed pocket celerity decreased as the thickness of the backward propagating front decreased, a result consistent with gravity current theory. The other extremity of the front did propagate as a curved gravity current front. One speculates that this type of pocket shearing may also be observed in deep stormwater storage tunnels laid in shallow slopes. This behavior was not observed for favorable slopes, when buoyancy forces oppose drag forces, as is explained below.

### 5.2 Air pocket spreading in adverse slopes

Results for adverse slopes (downstream end at a higher elevation than the upstream end) and no ambient flows are presented Figure 5.4. Trajectories and celerity values of the leading edge of the moving air pockets are shown for various volumes as well as various adverse pipeline slopes. The results do not present the curved trajectory from the air pocket leading edge that was present in horizontal cases even for the smallest slope tested of 0.5%. This indicates that air pocket spreading wasn't as pronounced and that the pocket leading edge was not significantly affected in the experiments. Another observation of this figure indicates the relative celerity difference between pocket of various volumes becomes less pronounced for larger pipeline slopes. That may indicate that larger slopes lead to more prominent concentration of air at the leading edge of the air pocket as it propagates, contributing to the reduction of these celerity values. Conversely, the pocket overall length for these smaller volume conditions was visibly shorter. Results for the smallest air pocket ($Vol^* = Vol/D^3$) and 2% show a much smaller celerity than corresponding cases with shallower slopes; this could be due to friction with pipeline walls which was more important for these small pocket volumes. However, for most tested cases, the relative celerity $C^* = C/\sqrt{gD}$ is limited by 0.47, which is consistent with results presented by [Baines(1991)].

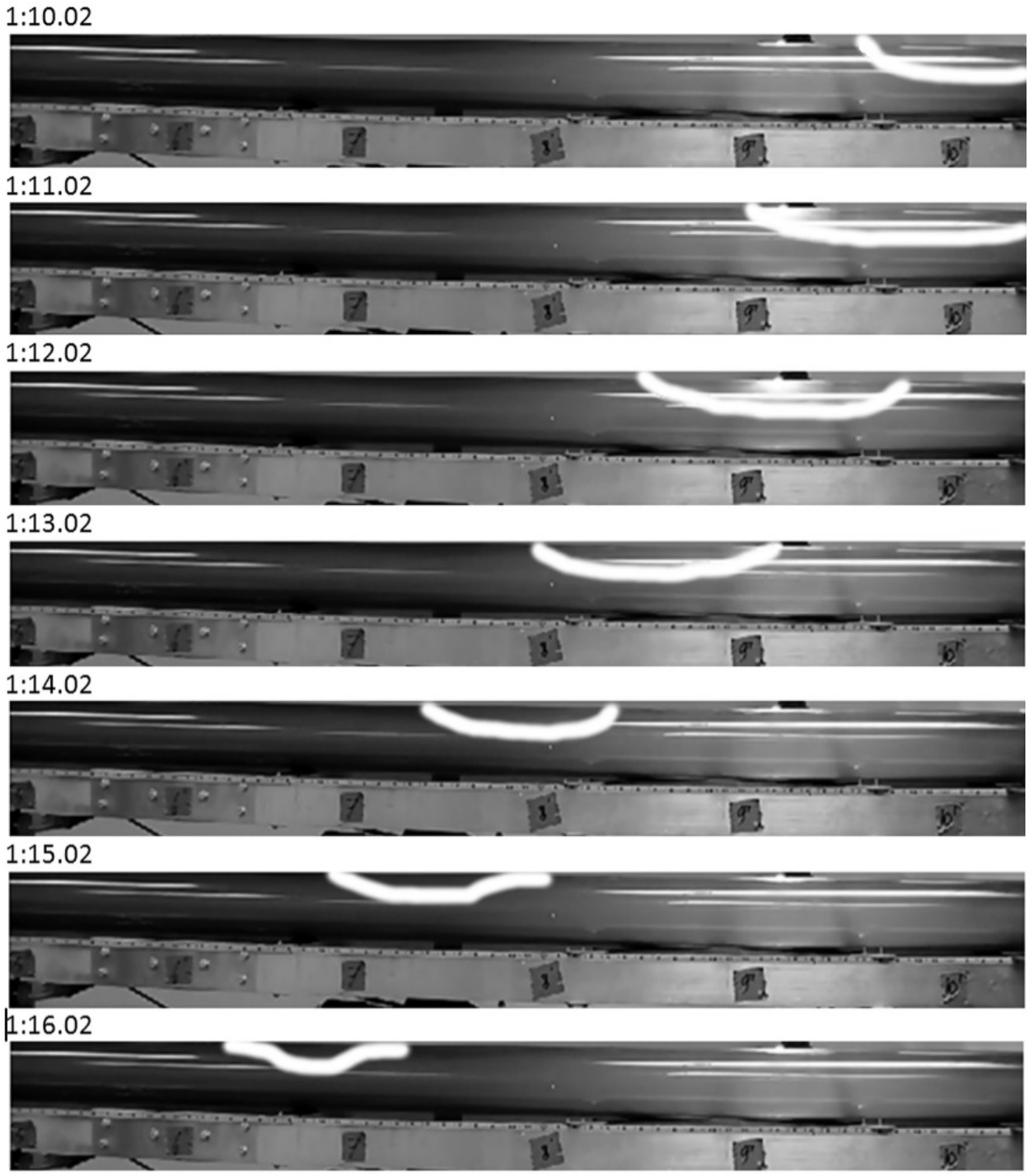


Figure 5.3: Sequence of snapshots illustrating the trajectory of the backward moving pocket trajectory for Q*=0.26, Vol*=4.1 and horizontal slope, illustrating the shearing process. Interface between air and water is enhanced.

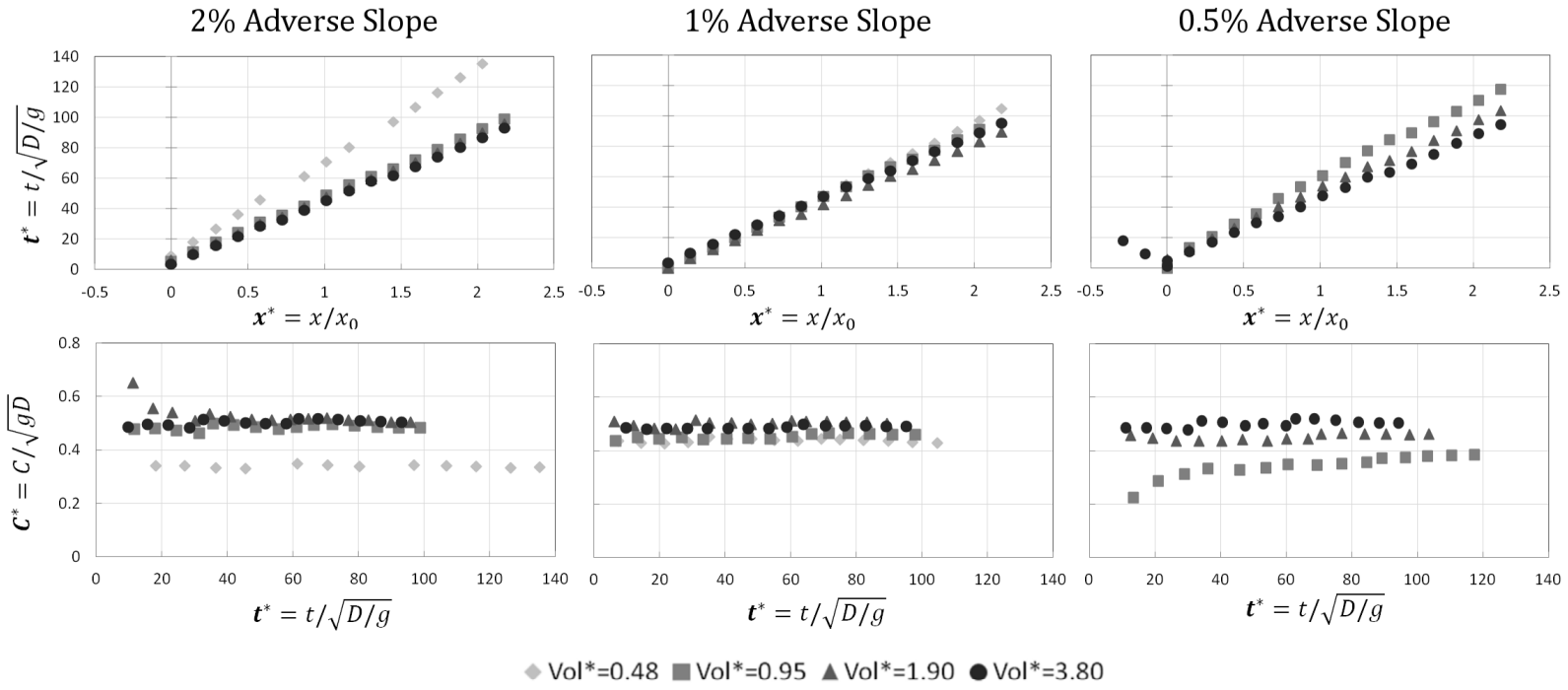


Figure 5.4: Trajectory of the air pocket leading edge and observed celerity for various adverse slopes and air pocket volumes, no ambient flow. Negative coordinates indicate pockets are propagating toward upstream.

Figure 5.5 presents the trajectories, observed celerity $C$ normalized by $\sqrt{gD}$, and the relative celerity accounting for ambient flow ($C$ - $v_{flow}$) also normalized by $\sqrt{gD}$, for the cases with $Vol^*$=0.95 and $Vol^*$=1.9 and 1% adverse slope. As anticipated, the observed air pocket front celerity increases with the flow rate, but changes in celerity between the two tested pocket volumes was comparatively smaller. In such slopes buoyancy and drag forces are summed and the air pocket celerity can also be approximated by the summation of the ambient flow velocity and the celerity observed in quiescent conditions. An exception to this observation was the case with $Vol^*$ =0.95 and the highest ambient flow $Q^*$ =0.37. An explanation of this observation is not available at this point.

### 5.3 Air pocket spreading in favorable slopes

This condition corresponded in the presence of ambient flow to the most complex case studied in this investigation due to the opposition between buoyancy and drag forces. Is it important to note that the conditions tested in this investigation did not involve flow rates that would promote the clearing of the pipeline (hydraulic clearing). The trajectories and celerities of the leading edge of the moving air pockets were plotted for various air pocket volumes and various favorable pipeline slopes without ambient flow. The results displayed in Figure 5.6 for all favorable sloped cases indicate little dependence on pipeline slope toward the trajectory for the largest pocket volume tested. As slope increased, the trajectory of the smaller pockets' leading edge approached that of the largest pocket; however, this was not the case for the smallest tested pocket of $Vol^*$=0.48, which was consistently slower. These findings are consistent with those presented by [Benjamin(1968)], indicating that for smaller pocket thickness celerity values should decrease significantly. Another notable observation is that for shallower slopes, air pockets spread over larger reaches of the pipeline. These results are qualitatively similar to those presented in Figure 5.4 for adverse slopes and no ambient flow. It should be noted that the detection of the back extremity of the air pocket was complicated by air pocket fragmentation into smaller pockets that was sometimes observed

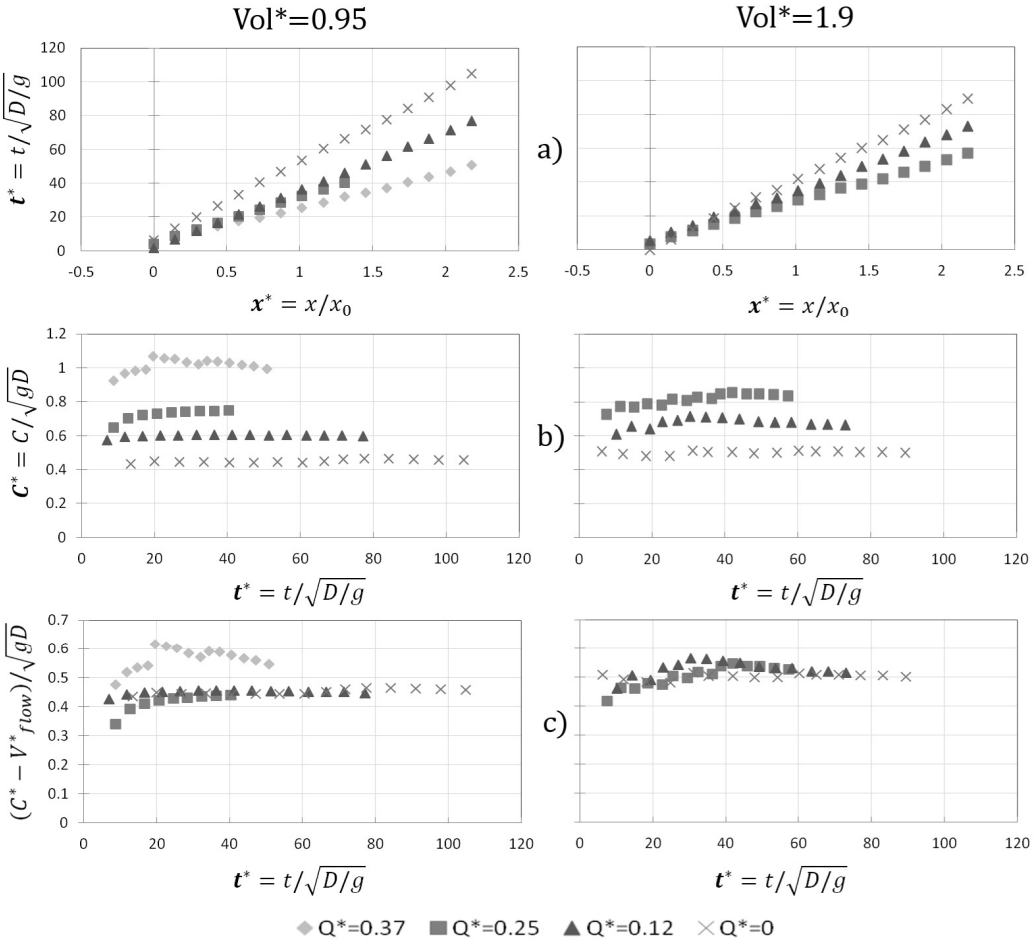


Figure 5.5: Trajectory of the air pocket leading edge, observed celerity and relative celerity for conditions with 1% adverse slope, ambient flow, and $Vol*$=0.95 and $Vol*$=1.9.

at these locations. Figure 5.7 shows a comparison between the front trajectories for adverse and favorable sloped conditions.

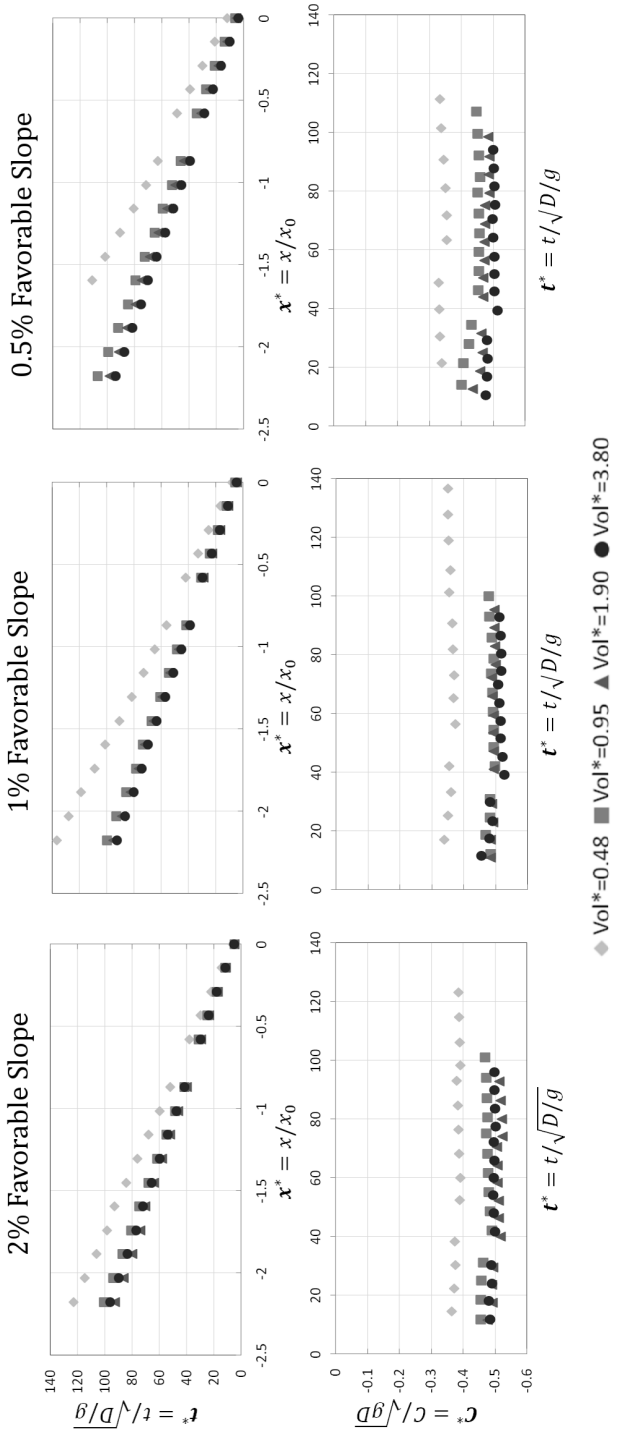


Figure 5.6: Trajectory of the air pocket leading edge and observed celerity for various favorable slopes and air pocket volumes, no ambient flow. Negative coordinates indicate pockets are propagating toward upstream.

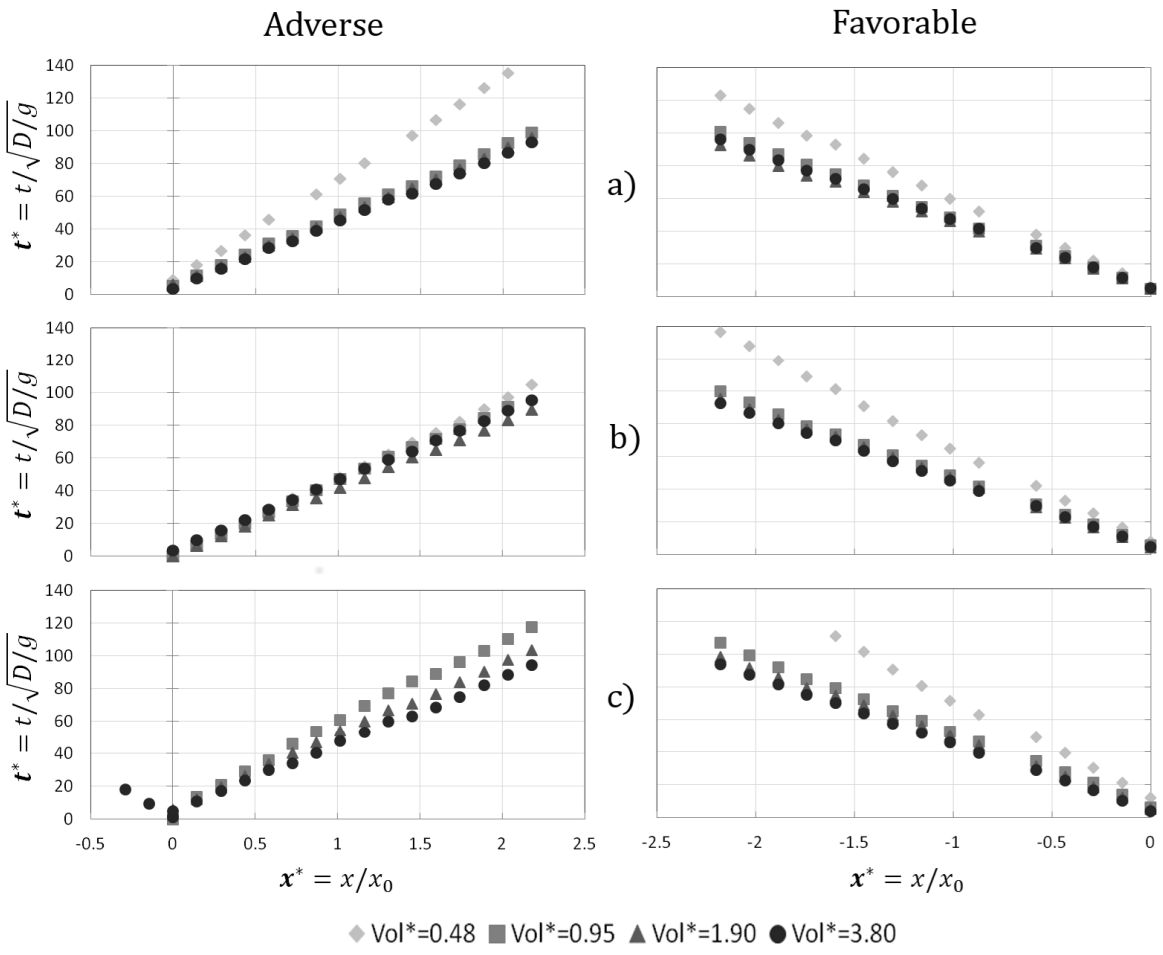


Figure 5.7: Trajectory of the air pocket leading edge for 2% (chart a), 1% (chart b) and 0.5% (chart c) adverse and favorable slopes and various air pocket volumes, no ambient flow. Negative coordinates indicate pockets are propagating toward upstream.

As mentioned, the most complex cases studied in this work involved favorable slopes with background flow, when buoyancy forces opposed drag forces. It was observed visually that the leading edge of the pockets advanced upstream against the ambient flow due to buoyancy in all tested slopes. Strong turbulence was observed at the trailing hydraulic jump behind the air pocket front. Air was sheared from the air pocket leading edge, but consistently with observations by [Pozos(2007)] and others, these smaller bubbles gathered downstream from the main pocket, and eventually grew in size and moved against the flow rejoining with the main pocket. This phenomenon is referred to as "blowback" by [Falvey(1980)] and others and has been linked to structural damage. A sample of these results is presented in Figure 5.8 that corresponds to the case where pocket volumes $Vol^*$=0.95 and $Vol^*$=1.9 and 1% favorable slope. Negative celerity values are due to the propagation direction of the pocket toward the upstream end of the apparatus. The observed celerity $C^*$ values for these favorable slopes, as anticipated, are smaller than the case with no ambient flow and ranged from -0.2 to -0.4 for all tested conditions. However, the assumption that these celerity values corresponded to the summation of celerity in quiescent conditions and the ambient flow conditions is no longer valid, a result that is likely linked to these complex air-water interactions observed in favorable slopes (e.g. shearing) that prevent pocket sizes to remain steady. These findings were consistent for all of the pocket volumes tested.

Figure 5.9 helps demonstrate this difference comparing the trajectories, observed celerity, and relative celerity accounting for ambient flow for the case when $Vol*$=1.9 and slope is either 1% adverse or 1% favorable. Appendix A presents example sets of experimental results for 0.5% favorable and adverse slopes with $Q^* \approx 0.12$, 0.25, and 0.37 as well as 2% favorable and adverse slopes with $Q^* \approx 0.12$, 0.25, and 0.37, which are very similar to those discussed in this previous section.

In summary, air pocket kinematics in favorable slopes and ambient flow conditions still demand further investigation. Due to the complexity of air-water interaction in such conditions, pocket volume varies and so does celerity. While the general assumption that observed

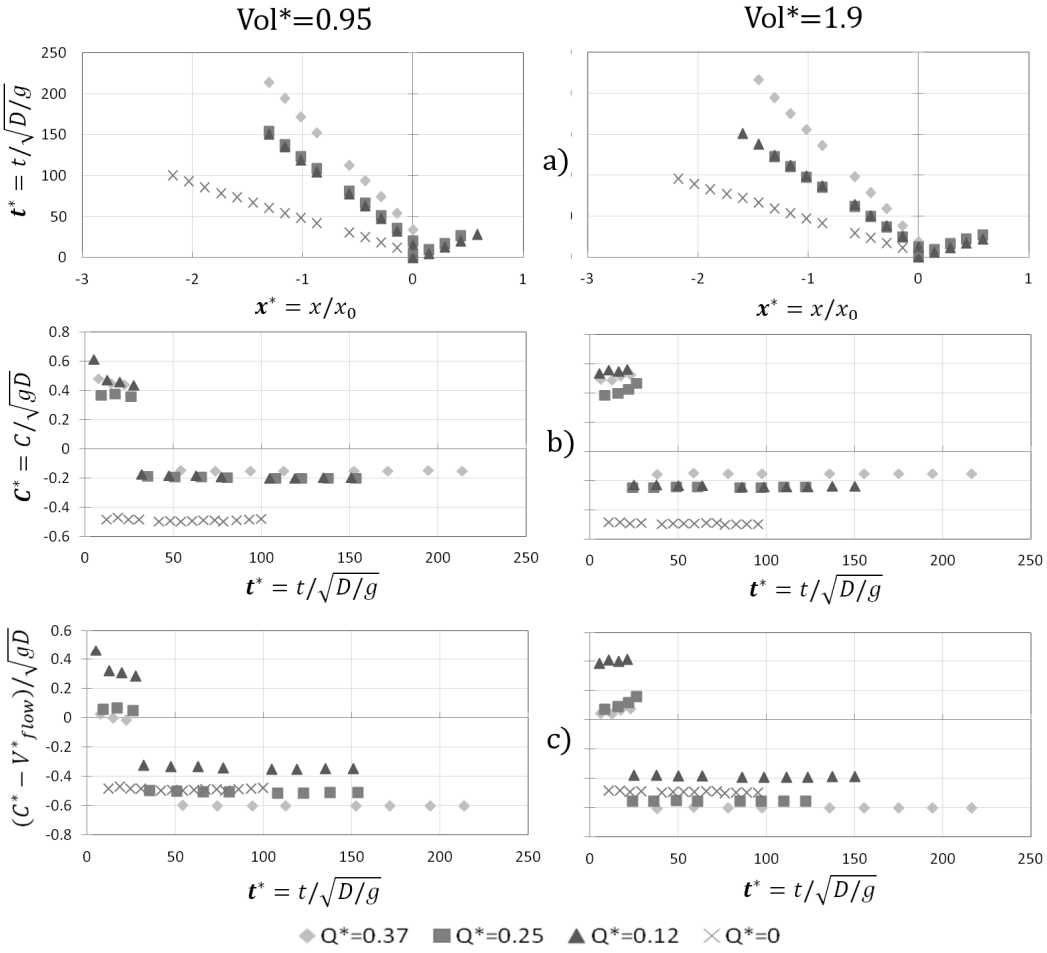


Figure 5.8: Trajectory of the air pocket leading edge, observed celerity and relative celerity for conditions with 1% favorable slope, ambient flow, and $Vol*$=0.95 and $Vol*$=1.9.

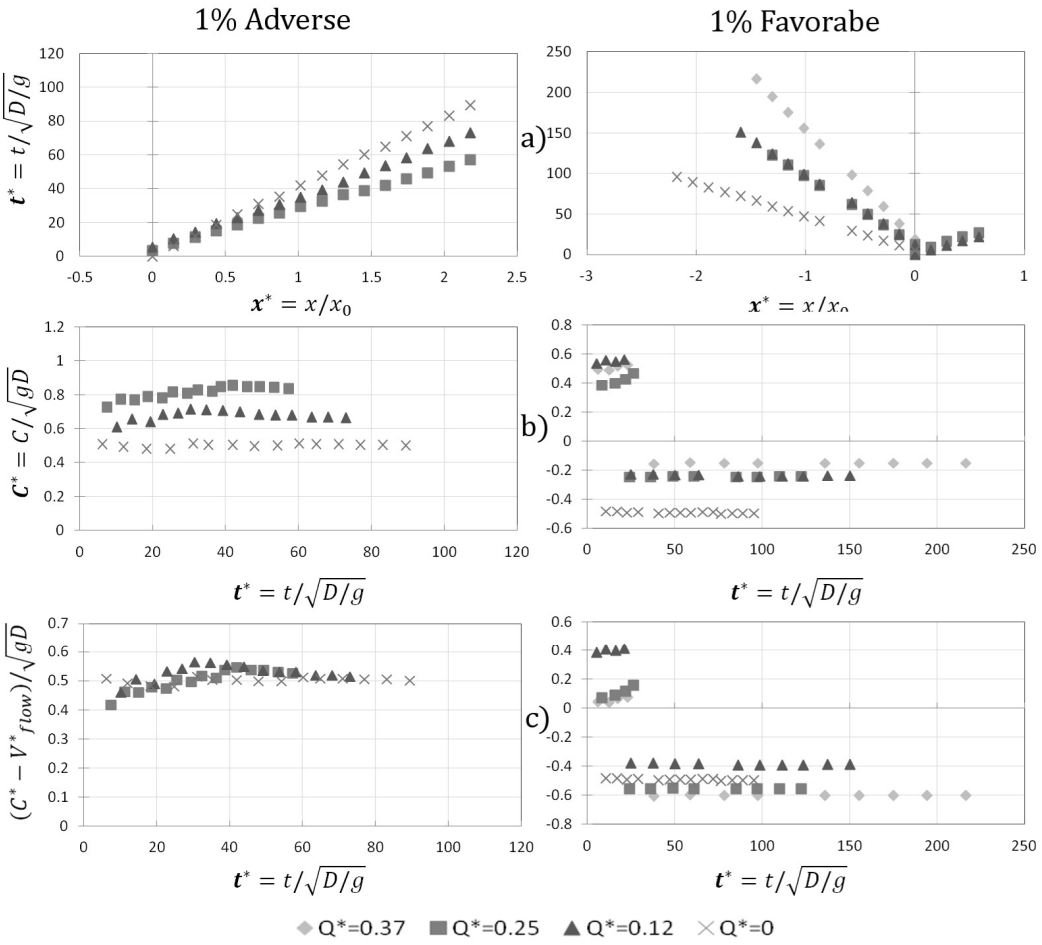


Figure 5.9: Trajectory of the air pocket leading edge (chart a), observed celerity (chart b) and relative celerity (chart c) for conditions with 1% adverse and 1% favorable slopes and ambient flow for $Vol*$=1.9.

celerity is not the summation of ambient flow velocity and pocket celerity in quiescent conditions, this relative celerity is in the range $-0.4$ and $-0.6$ for all tested cases. Larger scale studies should attempt to validate this estimate for relative celerity values.

## 5.4 Air pocket motion and spreading compared to numerical model prediction

A relevant question is to what extent can these experimental results be replicated by numerical models based on gravity current theory framework. Figure 5.10 shows the air pocket front trajectories simulated with both numerical models developed by Thomas Hatcher at

Auburn University (please see 4) for all horizontal flow experiments. The experimental results are greatly affected by background flow, and the effect of air pocket volumes on front velocity is also significant (boundary effects and surface tension are more important for smaller pocket volumes).

Without background flow, $M1$ performs better in comparison with experimental results. $M2$ consistently underestimates the air pocket leading edge celerity, and this underestimation increases for larger air pocket volumes. $M2$ is the more accurate model for the smallest air pocket volumes with background flow, although both models perform well. The accuracy of the $M1$ model seems to be unaffected by differing background flows and pocket volumes, which suggests that the surface tension parameters used by [Wilkinson(1982)] perform well for circular as well as rectangular cross-sections.

Both integral models over-predict the air pocket front velocity during the initial stages of simulation. This can be attributed to that fact that the formulations neglect the initial shear stresses caused and the anticipated local acceleration of water upon the complete opening of the knife gate valves that were keeping the air pocket in place. Once these shear stresses are no longer affecting the air pocket motion (at about $t^* \approx 20 - 30$), $M1$ slightly under-predicts the air pocket leading edge celerity, but $M2$ keeps providing a larger under-prediction.

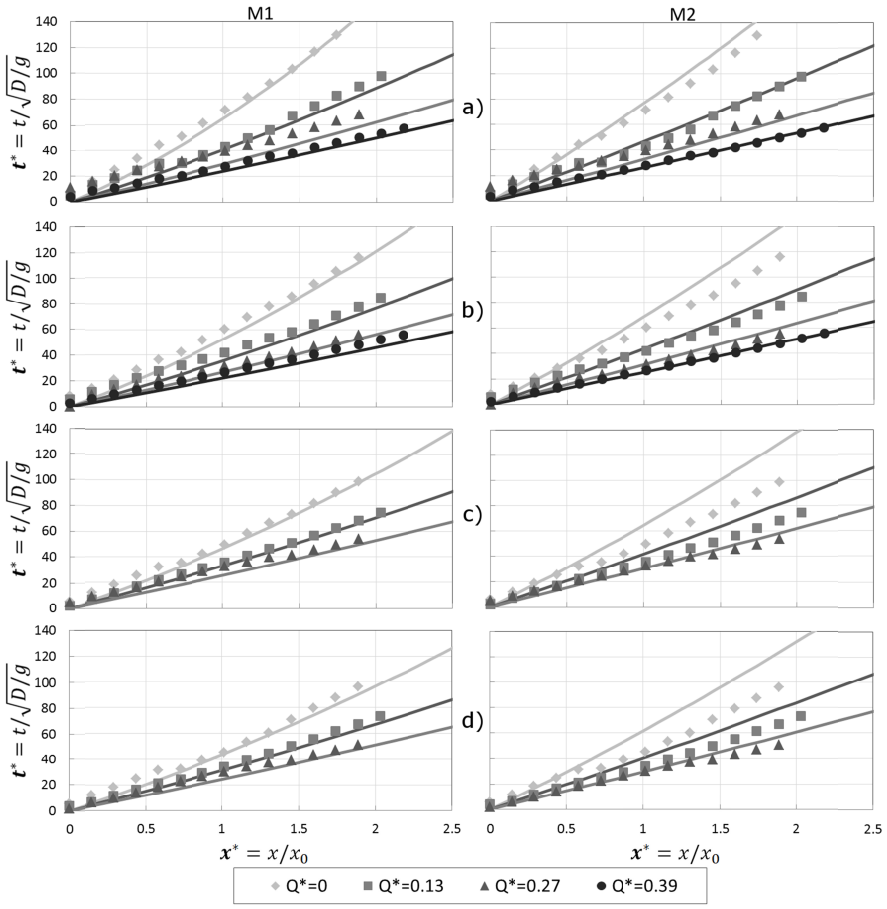


Figure 5.10: Air front trajectory comparison between experiments and both integral models for various background flows and pocket volumes: a) $Vol^* = 1.27$, b) $Vol^* = 2.22$, c) $Vol^* = 3.18$, and d) $Vol^* = 4.13$. The solid lines represent the integral model predictions, and the data markers represent experimental values.

# Chapter 6

## Conclusions and Future Work

This work presented results on an investigation of the motion of entrapped air pockets in water pipes. The focus was on the kinematic aspects of air pocket motion and air-water interactions related to the motion of these discrete, finite volume pockets. A long term goal of this research is to incorporate into flow regime transition models the ability to track entrapped pockets and prevent negative impacts related to these events in stormwater storage tunnels and transmission mains.

An experimental program was proposed where different conditions of pipe slope and ambient flow rates were tested. Use of clear PVC pipe enabled tracking the coordinates of entrapped pockets over time for each tested condition. In addition to the experimental studies, a non-Boussinesq, integral model was used to simulate some of the conditions tested in the experiments. The purpose of this gravity current model was the possibility of such a simple, computationally inexpensive modeling approach being included as a sub-model in a more complex flow regime transition model.

The findings of this research may be summarized as follows:

- The celerity of discrete air pockets in stagnant flow conditions depended on air pocket volume, particularly for shallower slopes (below 0.5%), in agreement with [Benjamin(1968)] and [Wilkinson(1982)] observations. For stronger slopes, celerity values were not as dependent on volumes as air accumulation at the leading edge of the air pocket reduced differences on the pocket thickness;

- For horizontal slope and stagnant conditions, the air pocket celerity values slightly decreased over time, indicating that the air pocket spreading decreased the leading edge thickness, resulting in smaller celerity values;

- It was observed that the propagation of air pockets in horizontal slope pipes against ambient flows is short lived due to the shearing of the air pockets in the hydraulic jumps that trailed the leading edge of the air pocket even when ambient velocities are smaller than air pocket celerity;

- In ambient flow conditions, the celerity of the air pocket leading edge in horizontal and adverse slopes was well approximated by the summation of celerity values in quiescent conditions and the ambient flow velocity. Such an approximation did not hold for air pocket propagation in favorable slopes where buoyancy forces opposed drag forces;

- Air pocket propagation in favorable slopes was slowed down by ambient flows, and shearing of the leading edge of the main air pocket by the trailing hydraulic jump was observed. However, these sheared bubbles regrouped in larger bubbles/pockets downstream from the main air pocket. As these bubbles grew to a certain size, they would have enough velocity to overcome the ambient drag and eventually rejoin the main air pocket.

- Predictions of the air pockets leading edge coordinate yielded by proposed numerical models compared fairly well with experiments with horizontal slopes, with and without ambient flow. The $M1$ model (based on the work of [Benjamin(1968)] and [Wilkinson(1982)]) yielded better results for large air pocket volumes and smaller ambient flows. The $M2$ model results were more accurate only for the smallest air pocket volumes ($Vol^* = 1.2$) and higher ambient flows.

This work also highlighted points that should be addressed in future investigations. One is the development of similar studies using other pipe diameters to assess scale effects on these findings. Experiments with 50 mm and 200 mm pipes are planned in the future to complement findings presented in this work. Experimental studies that involve both flow regime transition and entrapment of air pockets are also planned to help assess the effectiveness of such a combination in controlled laboratory conditions. Further numerical

investigations, including the use of computational fluid dynamics (CFD) packages, would also be useful.

Operational difficulties with the experimental setup that could be addressed in the future include: 1)development of uniform mechanism/procedure to close knife gate valves to keep the air pocket from moving before the beginning of each experimental run; 2) better system for opening both knife gate valves simultaneously to release the pocket in both the upstream and downstream directions; and 3) developing a mechanism that would allow small bubbles of air occasionally admitted from the upstream reservoir to be expelled prior to experimental runs.

It would also be helpful in the future to use all data collected during experimental runs. Pressure monitoring that occurred throughout the system can be used to assess the amount of energy loss caused by the partially closed knife gate valves holding the pocket in its initial position. Also, measurements of the air pocket thickness in selected cases would be valuable information since there is evidence in literature of the relationship between pocket thickness and celerity during motion.

Bibliography

[Aimable and Zech(2003)] Aimable, R. and Zech, Y. (2003). Experimental results on transient and intermittent flows in a sewer pipe model. *Proc. of 30th IAHR Congress, Vol. B, Thessaloniki, Greece*: 377–384, 2003.

[Baines(1991)] Baines, W.F. (1991). Air cavities as gravity currents on slope. *J. Hydr. Eng.*,**117**(12): 1600–1615, 1991.

[Barnea and Taitel(1993)] Barnea, D. and Taitel, Y. (1993). Model for slug length distribution in gas-liquid slug flow. *Int. J. Multiphase Flow*,**19**(5): 829–838, 1993.

[Benjamin(1968)] Benjamin, T.B. (1968). Gravity currents and related phenomena. *J. Fluid Mech.*, 31: 209–248, 1968.

[DeHenau and Raithby(1995)] DeHenau, V. and Raithby, G.D. (1995). Transient two-fluid model for the simulation of slug flow in pipelines. *Int. J. Multiphase Flow*,**21**(3): 335–349, 1995.

[DeMartino et al (2008)] De Martino, G., Fontana, N. and Giugni, M. (2008). Transient flow caused by air expulsion through an orifice. *J. Hydr. Eng.*,**134**(9): 1395–1399, 2008.

[Falvey(1980)] Falvey, H.T. (1980). Air-water flow in hydraulic structures. *USBR Engineering Monograph*, n. 41

[Gardner and Crow(1970)] Gardner, G.C. and Crow, I.G. (1970). The motion of large bubbles in horizontal channels. *J. Fluid Mech.*, **43**: 247–255, 1970.

[Glauser and Wickenhauser(2009)] Glauser, S. and Wickenhauser, M. (2009). Bubble movement in downward-inclined pipes. *J. Hydr. Eng.*, **135**(11): 1012–1015, 2009.

[Guo and Song(1991)] Guo, Q. and Song, C.S.S. (1991). Dropshaft hydrodynamics under transient conditions. *J. Hydr. Eng.*, **117**(8): 1042–1055, 1991.

[Hallworth et al(1998)] Hallworth, M.A., Hogg, A.J., and Huppert, H.E. (1998). Effects of external flow on compositional and particle gravity currents. *J. Fluid Mech.*, **359**: 109–142, 1998.

[Harris et al(2001)] Harris, T.C., Hogg, A.J. and Huppert, H.E. (2001). A mathematical framework for the analysis of particle-driven gravity currents. *Proc. R. Soc. Lond.*, **A**(457): 1241–1272, 2001.

[Hamam and McCorquodale(1982)] Hamam, M.A. and McCorquodale, A. (1982). Transient conditions in the transition from gravity to surcharged sewer flow. *Can. J. Civ. Engrg*, (9): 189–196, 1982.

[Hatcher et al(2013)] Hatcher, T.M., Chosie, C.D., and Vasconcelos, J.G. (2013). Modeling the motion and spread of air pockets within stormwater sewers. *CHI*, 2013.

[Issa and Kempf(2003)] Issa, R.I. and Kempf, M.H.W. (2003). Simulation of slug flow in horizontal and nearly horizontal pipes with the two-fluid model. *Int. J. Multiphase Flow*, **29**(1): 69–95, 2003.

[Kalinske and Bliss(1943)] Kalinske, A.A. and Bliss, P.H. (1943). Removal of air from pipe lines by flowing water. *Proc. Am. Soc. Civ. Eng. (ASCE)*, **13**(10), 1943.

[Kalinske and Robertson(1943)] Kalinske, A.A. and Robertson, J.M. (1943). Closed conduit flow. *Proc. Am. Soc. Civ. Eng. (ASCE)*, **108**: 1435–1447, 1943.

[Lauchlan et al(2005)] Lauchlan, C.S., Escarameia, M., May, R.W.P., Burrows, R. and Gahan, C.(2005). Air in pipelines - A literature review. *HR Wallingford Technical Report SR.*, 649.

[Lautenbach et al(2008)] Lautenbach, D. J., Vasconcelos, J. G., Wright, S. J., Wolfe, J. R., Cassidy, J. F. and Klaver, P. R. (2008). Analysis of transient surge in the proposed District of Columbia Water and Sewer Authority deep tunnel system. *Proc., 2008 WEF Collection Systems Conference, Pittsburgh, PA.*, 2008.

[Lautenbach and Klaver(2010)] Lautenbach, D. J. and Klaver, P. (2010). Experience of built tunnel systems with surges, transients and geysering. *Memorandum from LimnoTech Inc. to London Tideway Tunnels Delivery Team*, 2010.

[Li and McCorquodale(1999)] Li, J. and McCorquodale, A. (1999). Modeling Mixed Flow in Storm Sewers. *J. Hydr. Eng.*, **125**(11): 1170–1180, 1999.

[Lingireddy et al(2004)] Lingireddy, S., Wood, D.J. and Zloczower, N. (2004). Pressure surges in pipeline systems resulting from air releases. *J. AWWA*, **96**(7): 88–94, 2004.

[Little et al(2008)] Little, M.J., Powell, J.C. and Clark, P.B. (2008). Air movement in water pipelines - some new developments. *Proc., 10th Int. Conf. on Pressure Surges, BHR, Edinburgh, UK*, 111–122, 2008.

[Martin(1976)] Martin, C.S. (1976). Entrapped air in pipelines. *Proc., 2nd Int. Conf. on Pressure Surges, BHR, Bedford, England*, 15–28, 1976.

[Nielsen and Davis(2009)] Nielsen, K.D., and Davis, A.L. (2009). Air migration analysis of the Terror Lake tunnel. *Proc., 33rd IAHR Congress, IAHR, Vancouver, BC*, 262–268, 2009.

[Perron et al.(2006)] Perron, A., Kiss, L.I. and Poncsak, S. (2006). An experimental investigation of the motion of single bubbles under a slightly inclined surface. *Int. J. Multiphase Flow*, **32**: 606–622, 2006.

[Pinott and Moller(2011)] Pinott, M. and Moller, G. (2011). Intake structure of the Handeck 2 power plant (Switzerland), physical model investigation. *Swiss Federal Institute of Technology, Zurich*, 2011.

[Pothof and Clemens(2008)] Pothof, I. and Clemens, F. (2008). Air migration analysis of the Terror Lake tunnel. *Proc. 11th Int. Conf. Urban Drainage, Edinburgh, Scotland*, 2008.

[Pothof and Clemens(2010a)] Pothof, I. and Clemens, F. (2010). Interface drag on plugs in downward sloping pipes. *Proc. 7th Int. Conf. Multiphase Flows, Tampa, Florida*: 1–6, 2010.

[Pothof and Clemens(2010b)] Pothof, I. and Clemens, F. (2010). On elongated air pockets in downward sloping pipes. *J. Hydr. Res.*, **48**(4): 499–503, 2010.

[Pothof and Clemens(2012)] Pothof, I. and Clemens, F. (2012). Air pocket removal from downward sloping pipes. *Proc. 9th Int. Conf. Urban Drainage Modeling, Belgrade, Serbia*, 2012.

[Pozos(2007)] Pozos, O.E. (2007). Investigation on the effects of entrained air in pipelines. *PhD Thesis, University of Stuttgart*, 2007.

[Pozos et al(2010a)] Pozos, O., Giesecke, J., Marx, W., Rodal, E.A. and Sanchez, A. (2010). Experimental investigation of air pockets in pumping pipeline systems. *J. Hydr. Res.*, **48**(2): 269–273, 2010.

[Pozos et al(2010b)] Pozos, O., Gonzalez, C., Giesecke, J., Marx, W. and Rodal, E. (2010). Air entrapped in gravity pipeline systems. *J. Hydr. Res.*, **49**(3): 394–397, 2010.

[Simpson(1997)] Simpson, J.E. (1997). Gravity currents in the environment and the laboratory. *Cambridge University Press*, 1997.

[Song et al(1983)] Song, C.S.S., Cardle, J.A. and Leung, K.S. (1983). Transient mixed-flow models for storm sewers. *J. Hydr. Eng.*, **109**(11): 1487–1504, 1983.

[Toro(2009)] Toro, E. (2009). Riemann solvers and numerical methods for fluid dynamics: a practical introduction. *Springer Verlag*.

[Townson(1991)] Townson, J.M.(1991) Free-surface hydraulics. *Cambridge University Press*.

[Trindade and Vasconcelos(2013)] Trindade, B.C. and Vasconcelos, J.G. (2013) Modeling of water pipelines filling events accounting for air phase effects. *J. Hydr. Eng.*, (): 1943–7900, 2013.

[Vasconcelos and Leite(2012)] Vasconcelos, J.G. and Leite, G.M. (2012). Pressure surges following sudden air pocket entrapment in stormwater tunnels. *J. Hydr. Eng.*, **138**(12): 1080–1089, 2012.

[Vasconcelos and Wright(2006)] Vasconcelos, J.G. and Wright, S.J. (2006). Mechanisms for air pocket entrapment in stormwater storage tunnels. *Proc., 2006 ASCE EWRI Congress, Omaha, NE*, 2006.

[Vasconcelos and Wright(2008)] Vasconcelos, J.G. and Wright, S.J. (2008). Rapid flow startup in filled horizontal pipelines. *J. Hydr. Eng.*, **134**(7): 984–992, 2008.

[Vasconcelos and Wright(2009)] Vasconcelos, J.G. and Wright, S.J. (2009). Rapid filling of poorly ventilated stormwater storage tunnels. *J. Hydr. Res.*, **47**(5): 547–558, 2009.

[Vasconcelos and Wright(2011)] Vasconcelos, J.G. and Wright, S.J. (2011). Geysering generated by large air pockets released through water-filled ventilation shafts. *J. Hydr. Eng.*, **135**(5): 543–555, 2011.

[Wickenhauser and Kriewitz(2009)] Wickenhauser, M. and Kriewitz, C.R. (2009). Air-water flow in downward inclined large pipes. *Proc., 33rd IAHR Congress, IAHR, Vancouver, BC*, 5354–5361, 2009.

[Wilkinson(1982)] Wilkinson, D.L. (1982). Motion of air cavities in long horizontal ducts. *J. Fluid Mech.*, 118: 109–122, 1982.

[Wright et al(2011)] Wright, S.J., Lewis, J.W. and Vasconcelos, J.G. (2011). Geysering in rapidly filling storm-water tunnels. *J. Hydr. Eng.*, **137**(5): 543–555, 2011.

[Zhou et al(2002)] Zhou, F., Hicks, F.E. and Steffler, P.M. (2002). Transient flow in a rapidly filling horizontal pipe containing trapped air. *J. Hydr. Eng.*, **128**(6): 625–634, 2002.

[Zukoski (1966)] Zukoski, E.E. (1966). Influence of viscosity, surface tension, and inclination angle on motion of long bubbles in closed tubes. *J. Fluid Mech.*, **25**(4): 821–837, 1966.

# Appendices

# Appendix A

## Additional Experimental Results for Trajectory and Celerity

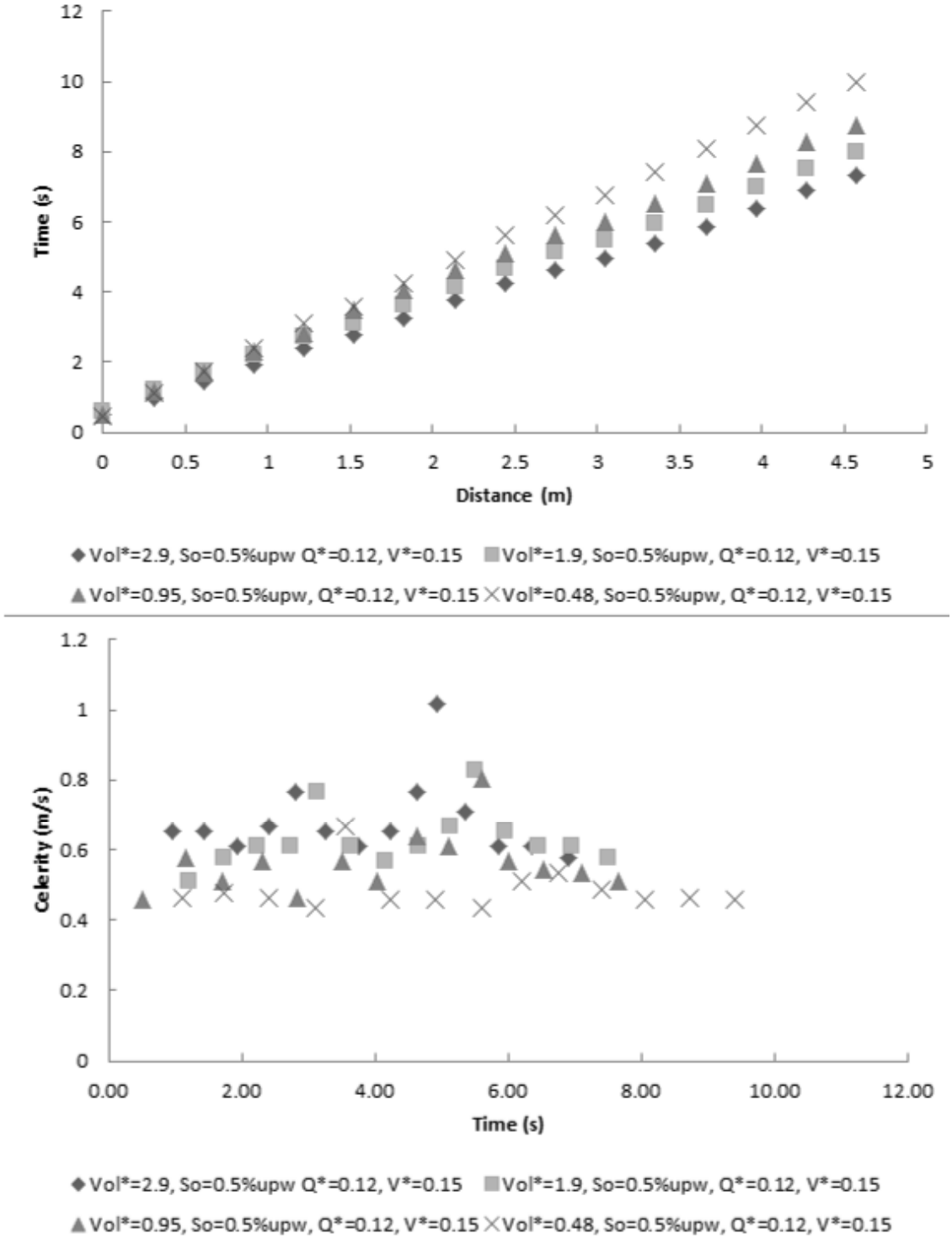


Figure A.1: Trajectory and celerity for 0.5% adverse slope and $Q^* \approx 0.12$.

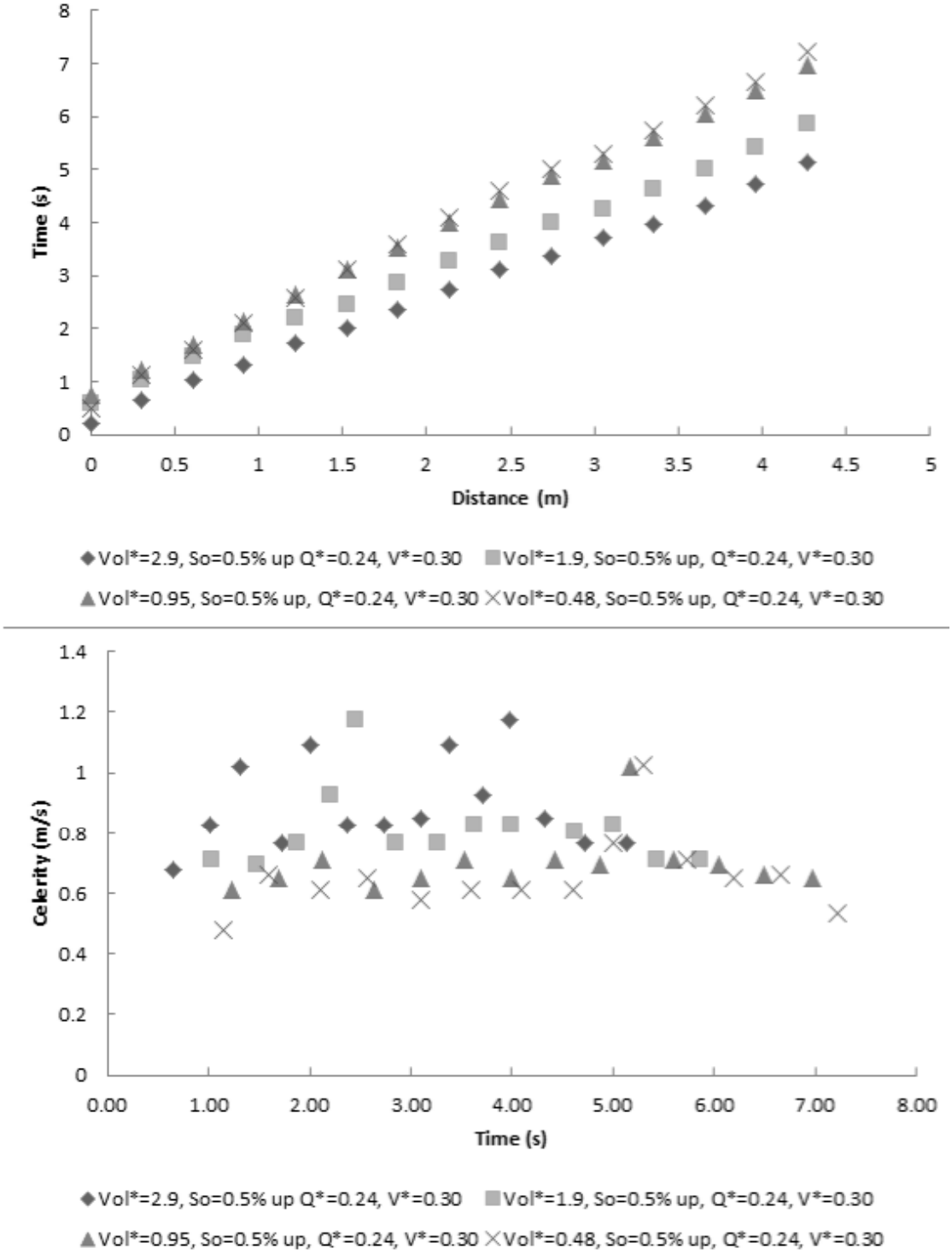


Figure A.2: Trajectory and celerity for 0.5% adverse slope and $Q^* \approx 0.25$.

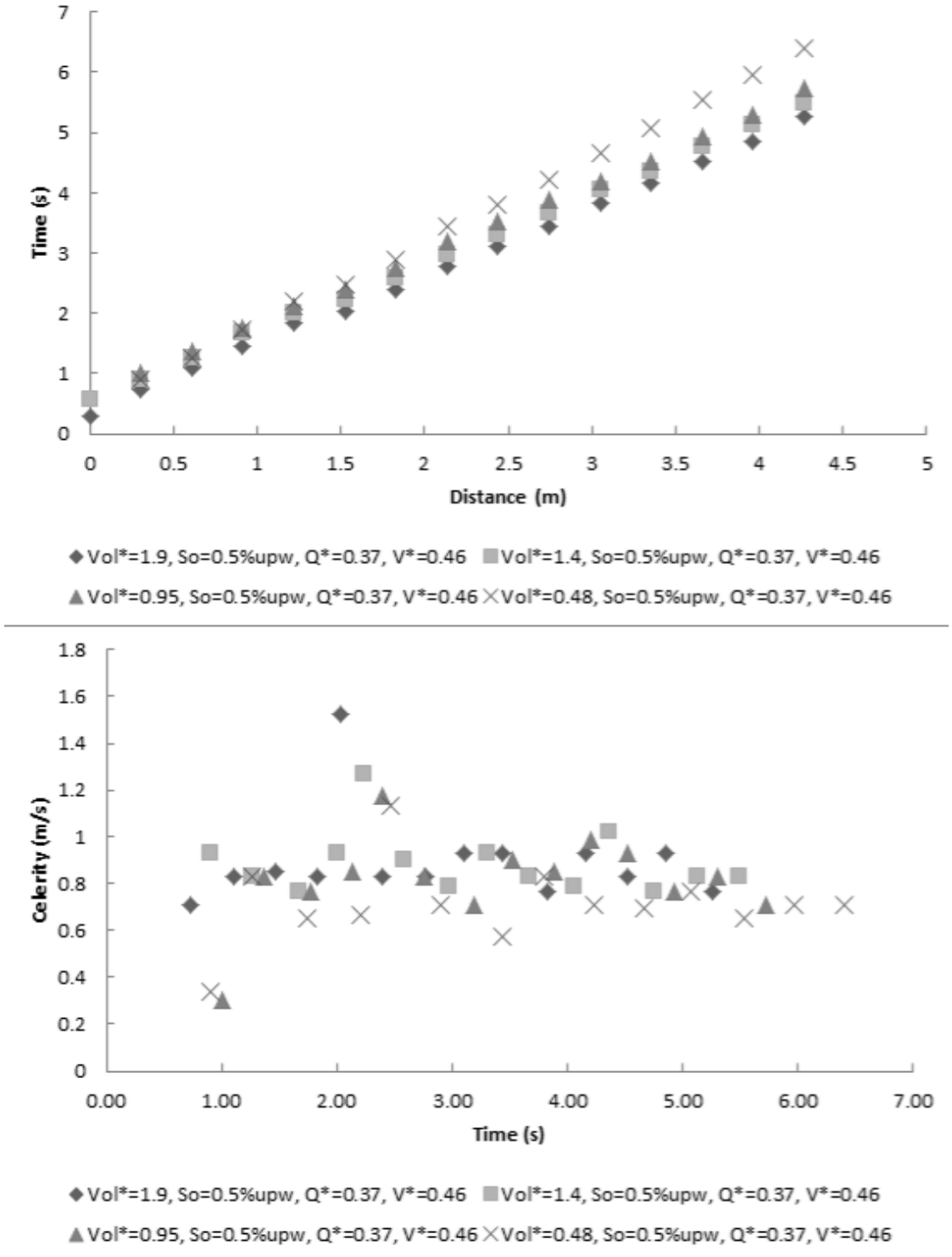


Figure A.3: Trajectory and celerity for 0.5% adverse slope and $Q^* \approx 0.37$.

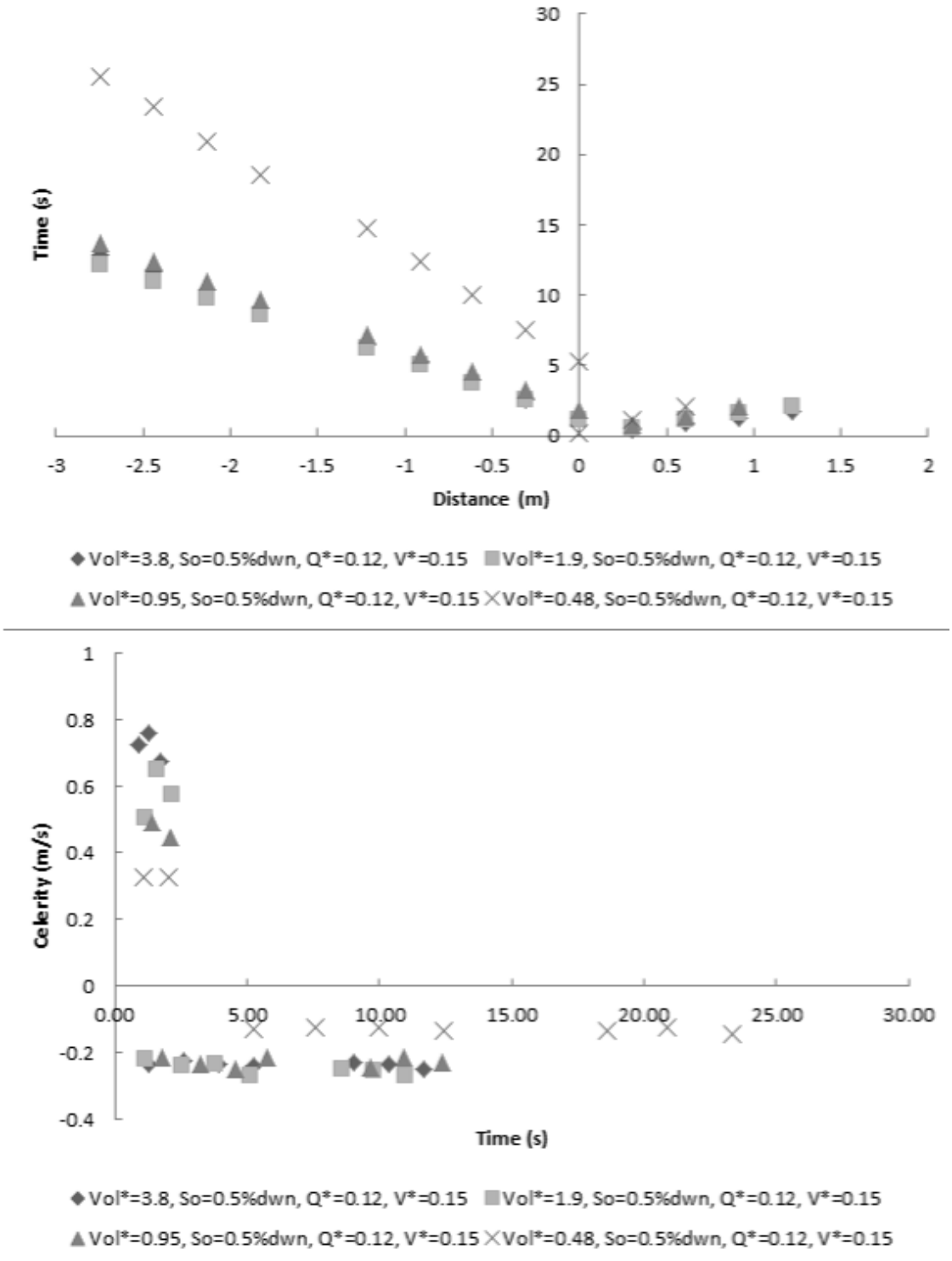


Figure A.4: Trajectory and celerity for 0.5% favorable slope and $Q^* \approx 0.12$.

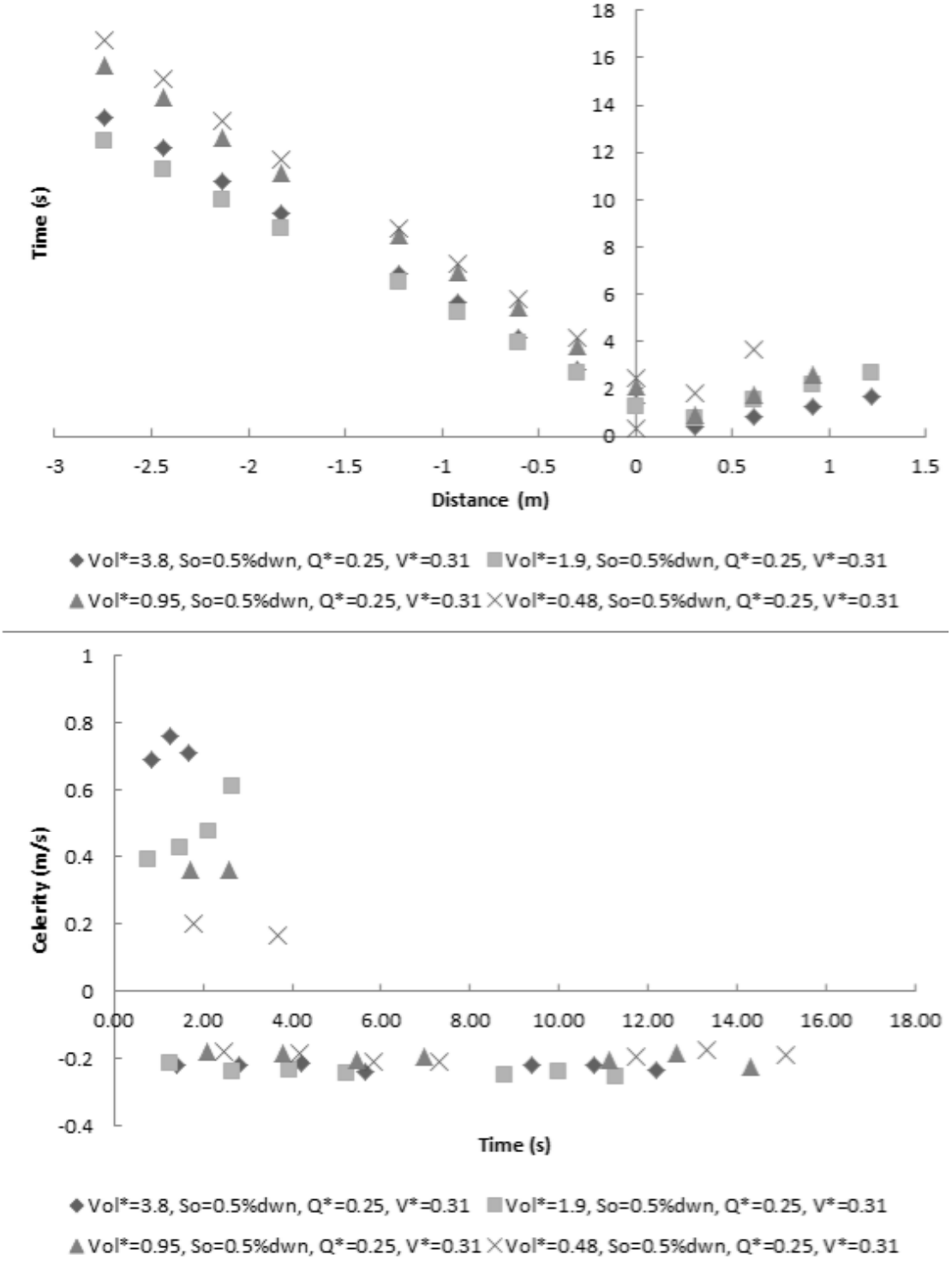


Figure A.5: Trajectory and celerity for 0.5% favorable slope and $Q^* \approx 0.25$.

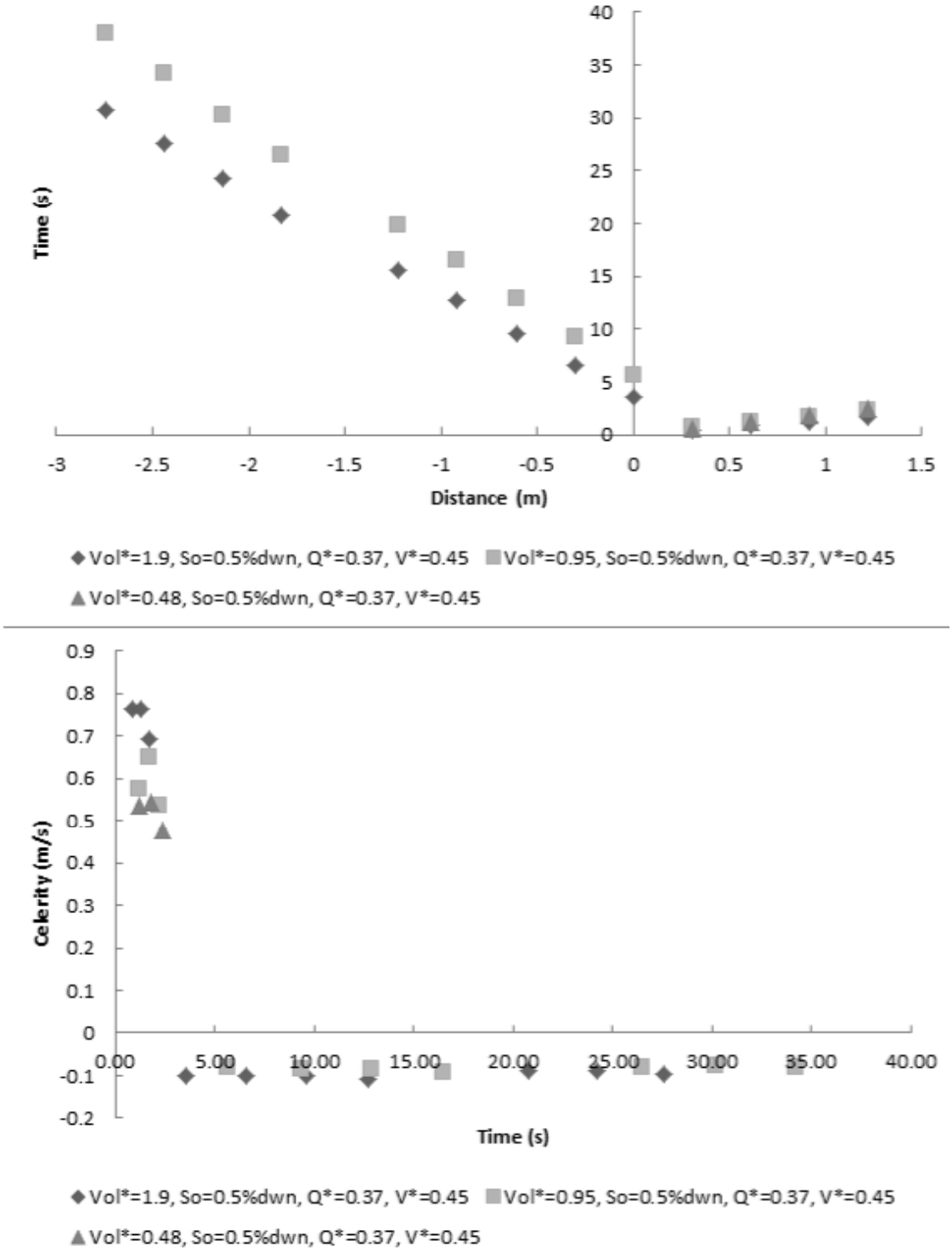


Figure A.6: Trajectory and celerity for 0.5% favorable slope and $Q^* \approx 0.37$.

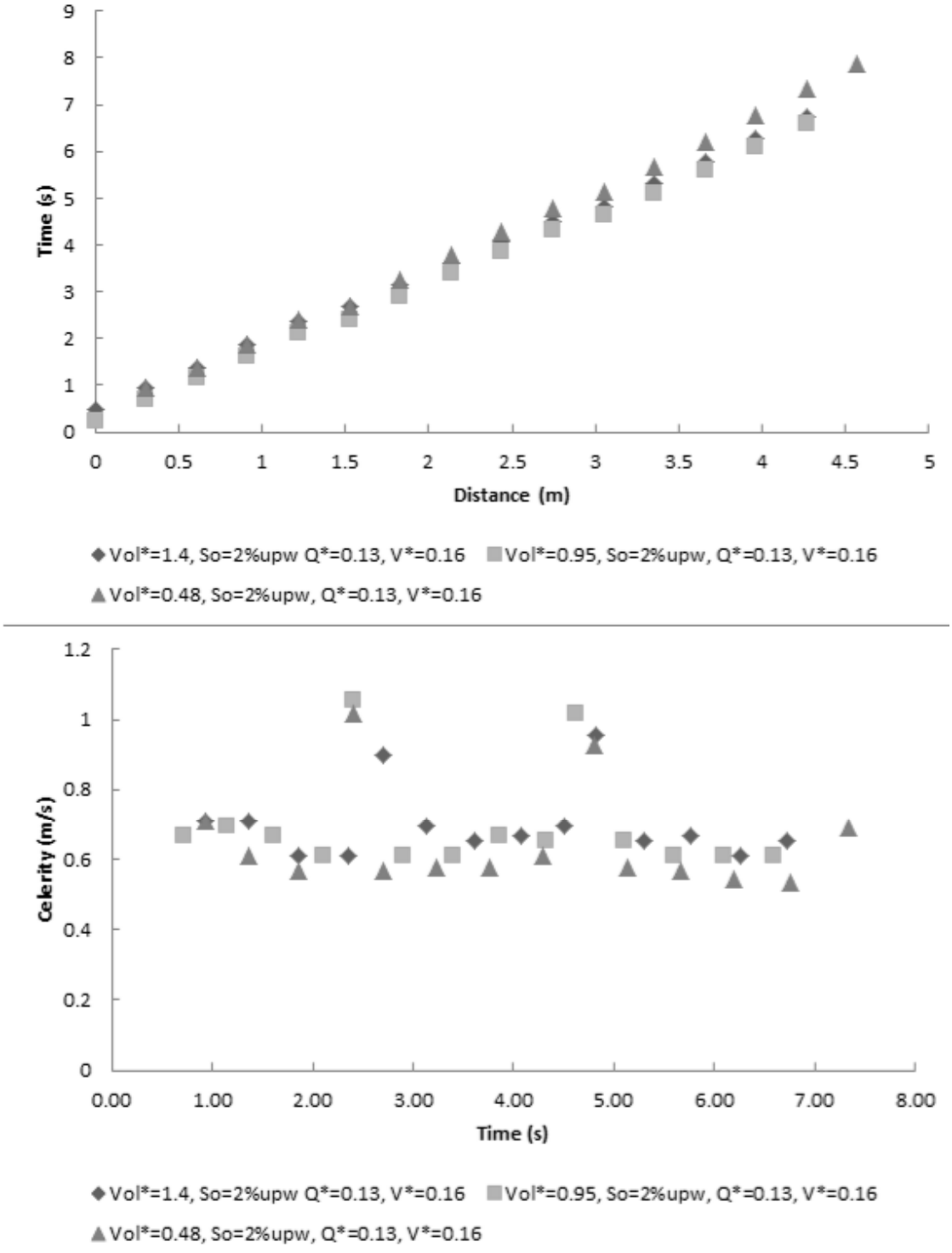


Figure A.7: Trajectory and celerity for 2% adverse slope and $Q^* \approx 0.12$.

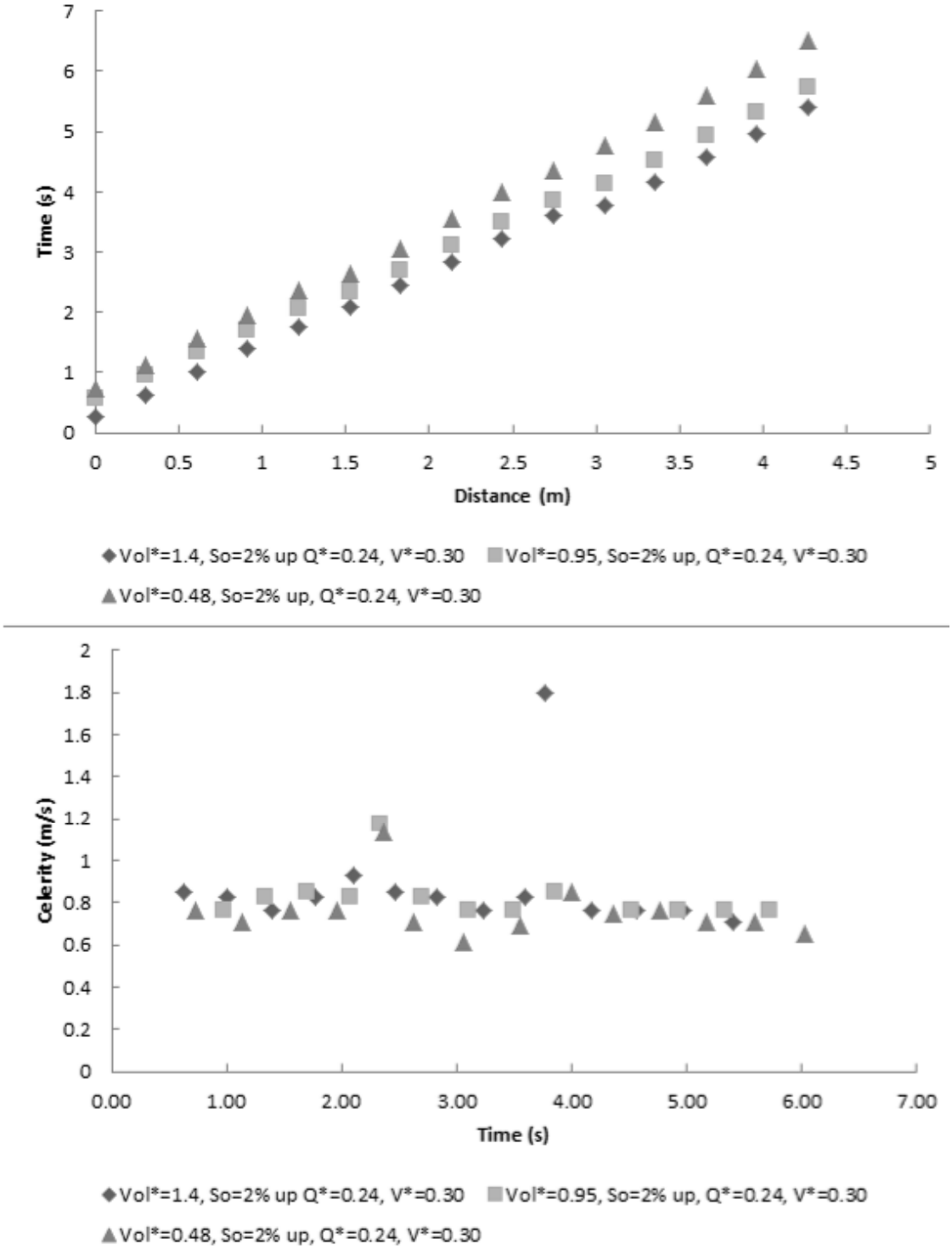


Figure A.8: Trajectory and celerity for 2% adverse slope and $Q^* \approx 0.25$.

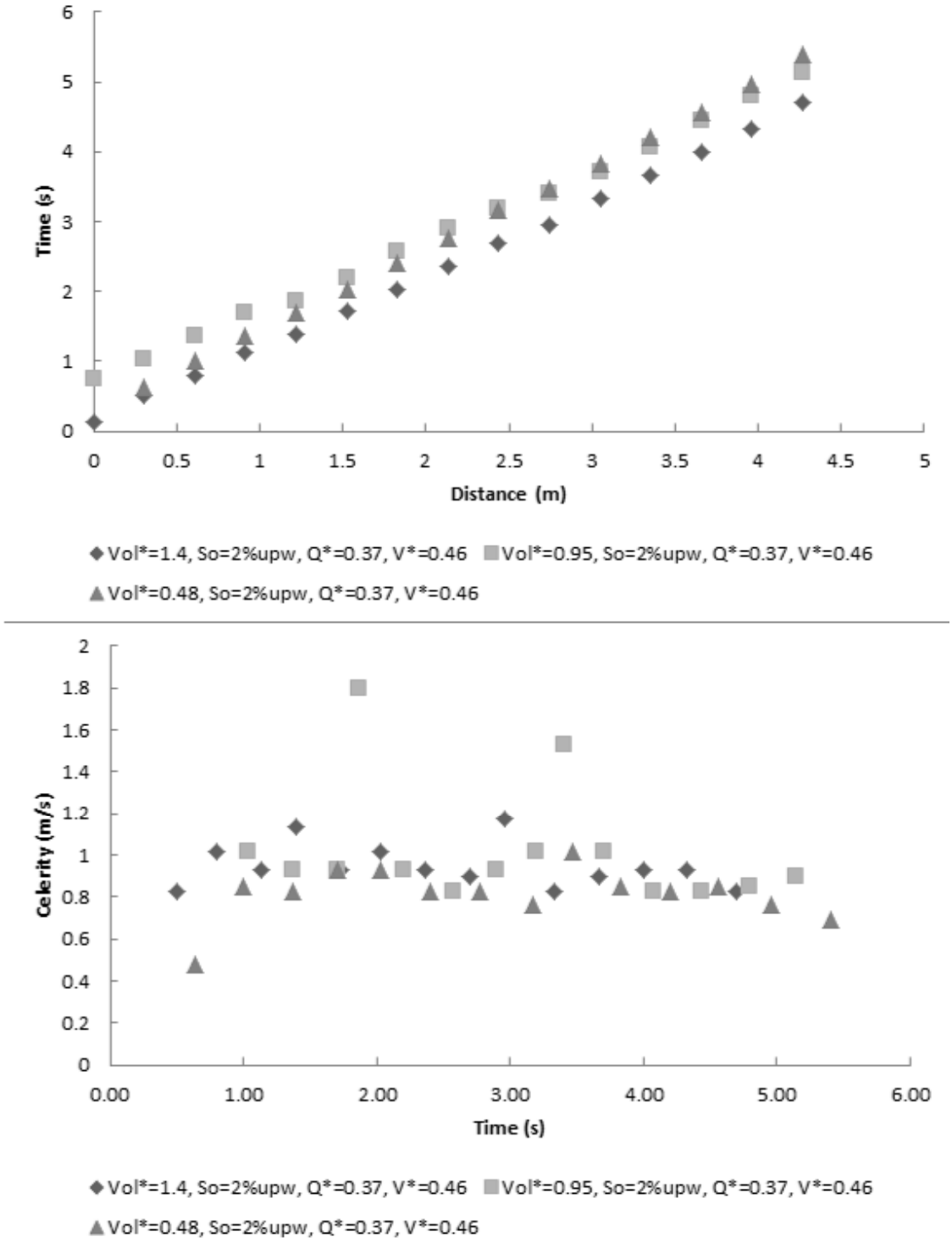


Figure A.9: Trajectory and celerity for 2% adverse slope and $Q^* \approx 0.37$.

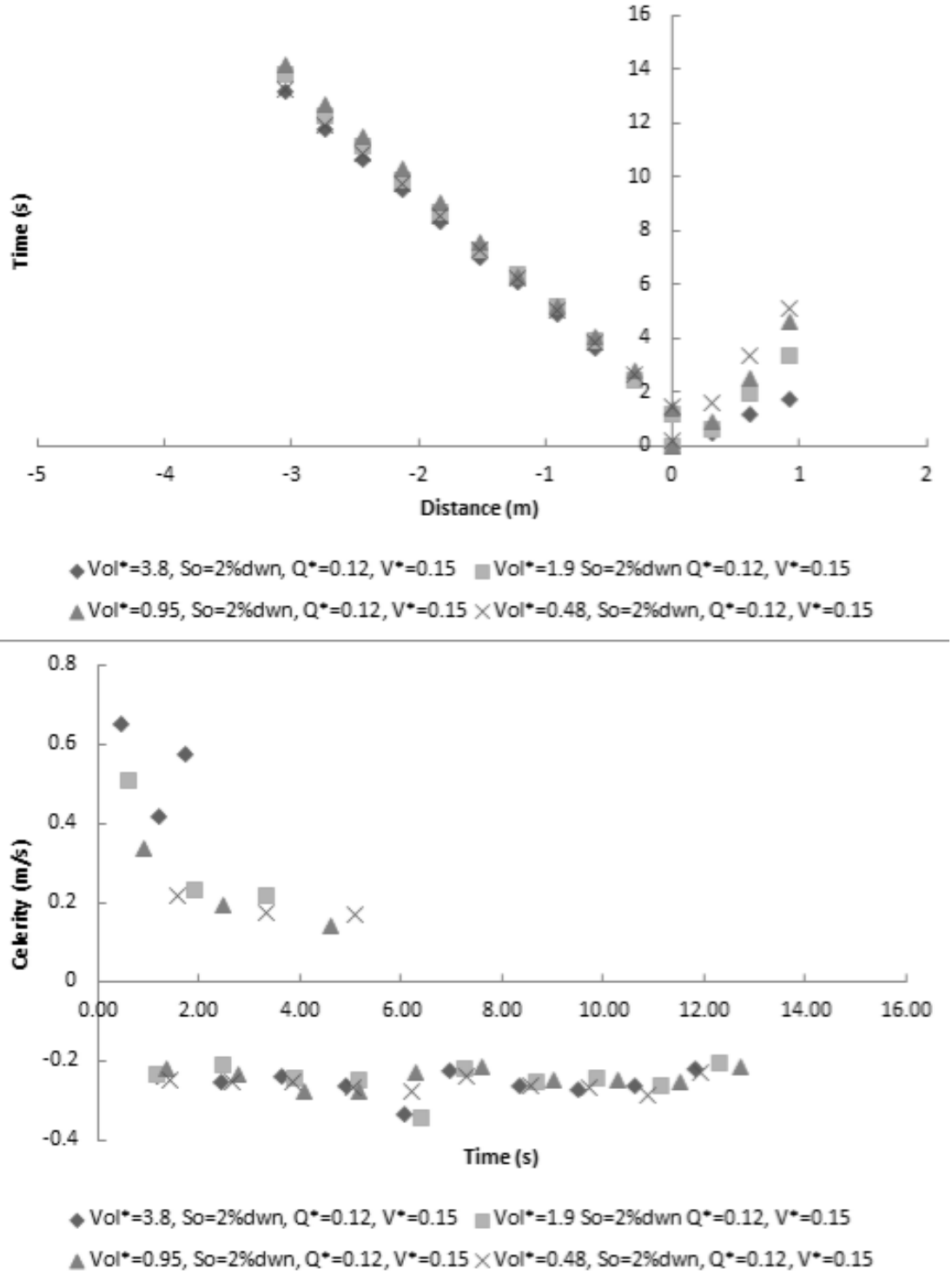


Figure A.10: Trajectory and celerity for 2% favorable slope and $Q^* \approx 0.12$.

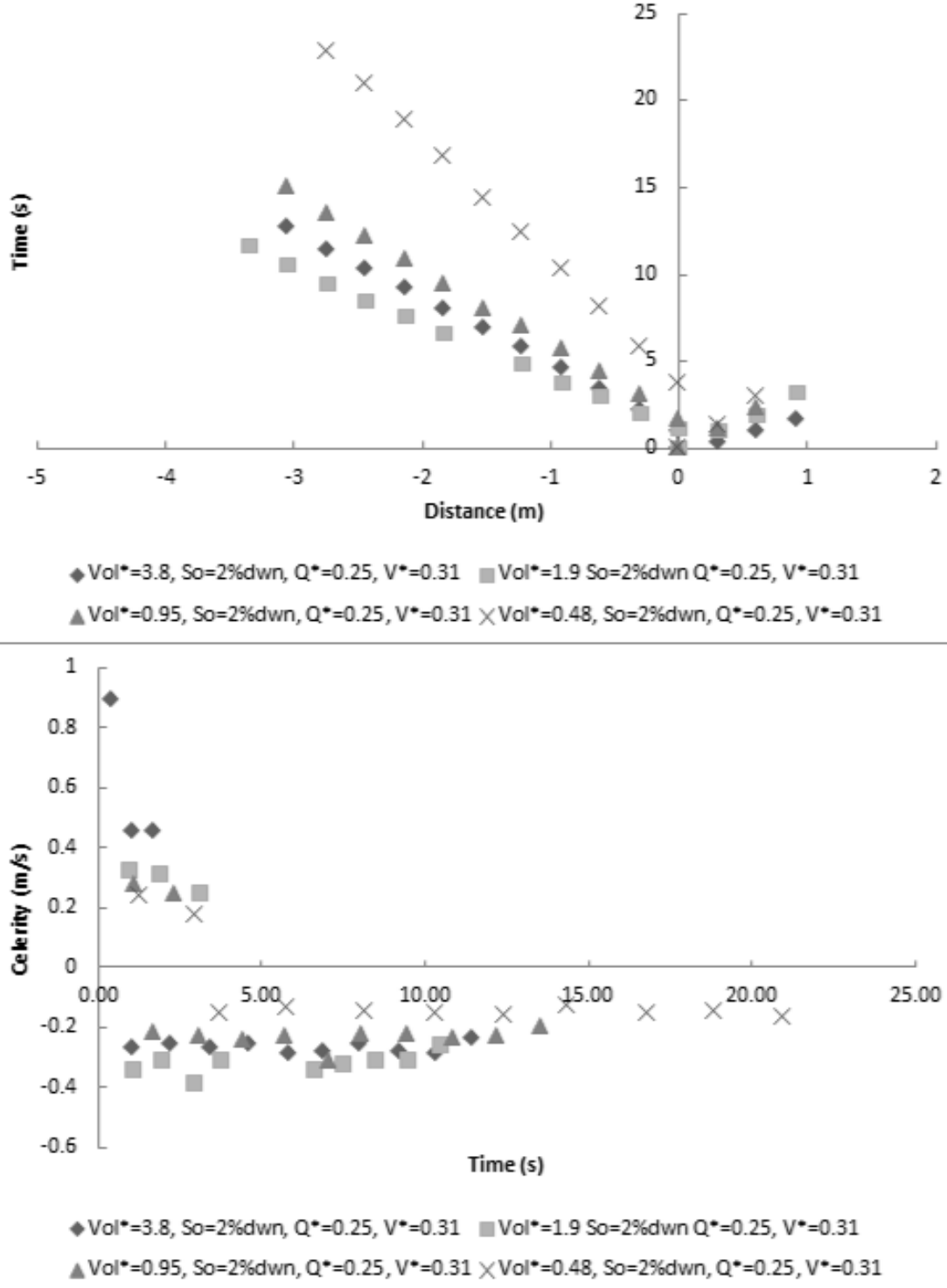


Figure A.11: Trajectory and celerity for 2% favorable slope and $Q^* \approx 0.25$.

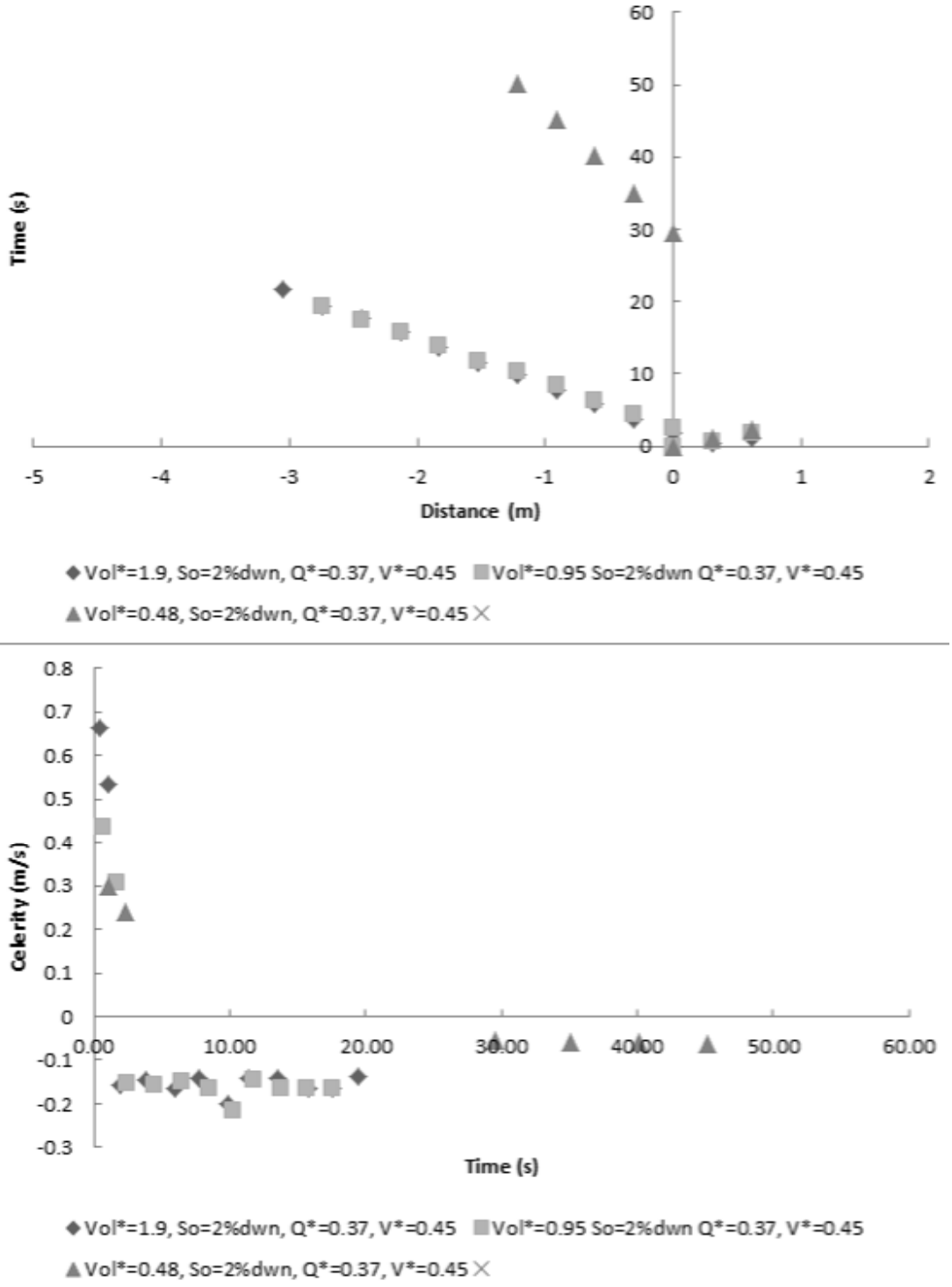


Figure A.12: Trajectory and celerity for 2% favorable slope and $Q^* \approx 0.37$.